Measurements and Modeling of Size Distributions, Settling and Dispersions (turbulent diffusion) Rates

A Final Report Submitted to

The Coastal Response Research Center

Submitted by

Dr. Joseph Katz
Department of Mechanical Engineering
Johns Hopkins University
3400 N Charles Street,
Baltimore, Maryland, 21218

Project Period: 1.1.2007 – 12.31.2008

March 13, 2009

Revised: August 31, 2009

Coastal Response Research Center

This project was funded by a grant from NOAA/UNH Coastal Response Research Center. NOAA Grant Number(s): NA 04 NOS 4190063. Project Number: 07-059

UNIVERSITY of NEW HAMPSHIRE

NOAA NATIONAL OCEANIC AND ATMOSPHERIC ADMINISTRATION U.S. DEPARTMENT OF COMMERCE

Abstract

The objective this project is to measure and parameterize the effects of turbulence and oil properties on the mean settling velocity, dispersion (turbulent diffusion) rate, and characteristic size distributions of oil droplets in water. These data are essential for modeling and predicting the dispersion rate of oil spills treated with dispersants. The first part of this project deals with measurements of dispersion rate and settling velocity of research grade diesel oil droplets. These measurements have been performed in a specialized laboratory facility that enables generation of carefully controlled, isotropic, homogeneous turbulence at a wide range of fully characterized intensities and length scales, covering most turbulence levels that one may expect to find in coastal waters. Oil droplets are injected into the sample volume, and their three-dimensional trajectories are measured at high resolution using high-speed digital holographic cinematography. An automated tracking program has been used for measuring velocity time history of more than 17,000 droplets with diameters ranging between 0.5-1.2 mm, and 15000 neutrally buoyant, 50 μm particles. The turbulent diffusion coefficient or dispersion rate of droplets in turbulence is calculated by integration of the ensemble averaged Lagrangian velocity auto-covariance. Trends of the asymptotic droplet diffusion coefficient are examined by viewing it as a product of a mean square velocity and a diffusion time scale. To compare the effects of turbulence and buoyancy, the turbulence intensity (u_i') is scaled by the droplet quiescent rise velocity (U_q). The droplet diffusion coefficients in horizontal and vertical directions are lower than those of the fluid at low normalized turbulence intensity, but exceed it with increasing normalized turbulence intensity. For most of the present conditions the droplet horizontal diffusion coefficient is higher than that in the vertical direction. The droplet diffusion coefficients scaled by the product of turbulence intensity and an integral length scale is a monotonically increasing function of u_i'/U_q. Using this scaling, empirical equations for the dispersion of oil droplet have been developed. Similar procedure is adopted to measure the diffusion coefficient of 35-70 μm oil droplets, and result is found to be similar to that of neutrally buoyant particles.

The second part of this project involves observations and measurements of the breakup process of crude oil mixed with the dispersant COREXIT 9527 at various dispersant to oil ratios. Breakups are visualized in the turbulent facility using high-speed digital holographic cinematography, which provide detailed description of the processes involved and the size distribution of droplets. Two different breakup mechanisms are identified. The first involves familiar capillary instabilities, and generates droplets that are typically larger than 100 μm. The second process, which generates droplets smaller than 5 μm, involves formation of very long, self-sustaining micro-threads extending from much larger droplet. Similar micro-threads form when the droplets are transported in a turbulent flow, when they are injected into quiescent fluid, and when a surface oil film is impinged by a water jet. Persistent breakup of these micro-threads may explain the formation of micro-droplets due to the addition of dispersants and possibly extend its usage beyond current scenarios.

Keywords

Turbulence, Droplets, Dispersion, Diffusion, Oil Spill, Dispersants, Breakup, Holography

Acknowledgments

This project was funded by a grant from NOAA/UNH Coastal Response Research Center, NOAA Grant Number(s): XXXXXXX, Project Number: 07-059. Early phases of this research were performed under a Department of Energy Grant No. DE-FG02-03ER46047. Graduate Students Balaji Gopalan and Siddarth Talapatra were involved in performing of experiments, data analysis and interpretation the results. Yury Ronzhes, our group engineer, was involved in design of experimental setup and maintenance of facilities.

Table of Contents

1.0		**Introduction**	7
2.0		**Objectives**	9
3.0		**Methods**	9
	3.1	Facility Description	9
	3.2	Turbulence Characterization	9
	3.3	Sample Preparation and Characterization	10
	3.4	Droplets and Fluid Dispersion Measurements	12
	3.5	Tracking of Oil Droplets and Fluid Particles	13
	3.6	Calculation of Diffusion Parameters	16
	3.7	Dimensional Analysis of Dispersion Coefficient	17
	3.8	Droplet Breakup Visualization	18
	3.9	Visualization of Droplets in Quiescent Flow and Impinged Surface	18
4.0		**Results**	19
	4.1	Transport of Diesel Oil Droplets	19
	4.1.1	Mean Rise Velocity	20
	4.1.2	PDF of Velocity Fluctuations	21
	4.1.3	Droplet Velocity Rms	21
	4.1.4	Scaling of Droplet Diffusion Coefficient	23
	4.1.5	Droplet Diffusion vs. Fluid Diffusion	28
	4.1.6	Dispersion of Extremely Small Oil Droplets	28
	4.1.7	Oil Droplet Mean Square Displacement	29
	4.2	Crude Oil Droplet Breakup	30
	4.2.1	Qualitative Analysis of Droplet Breakup Process	31
	4.2.2	Size Distribution Associated with Capillary Droplet Breakup	33
	4.2.3	Formation and Breakup of Droplet Threads in Turbulent and Quiescent Flow	34
	4.2.4	Connection to Actual Oil Spill Scenario	37
5.0		**Importance to Oil Spill Response/Restoration**	38
6.0		**Technology Transfer**	39
7.0		**Achievement and Dissemination**	39
8.0		**References**	40

List of Figures and Tables

Figure 1	Turbulence generating facility with the optical setup of one view digital holography.	10
Figure 2	Surface tension measurement using capillary tubes.	12
Figure 3	A sample (a) 2-D projection and (b) 3-D matched droplet tracks with grayscale showing velocity magnitude.	14
Figure 4	Sample ensemble averaged droplet Lagrangian velocity autocorrelations at Re_λ = 214.	16
Figure 5	Fluid and droplet (different sizes) horizontal diffusion coefficient as a function of time for (a) Re_λ = 190 (low u_i'/U_q) and (b) Re_λ = 214 (high u_i'/U_q)	18
Figure 6	Visualization experiments in quiescent flow.	19
Figure 7	Droplet mean rise velocity normalized by the quiescent rise velocity as a function of Stokes number. The corresponding Re_λ are 190, 195 and 214.	20
Figure 8	Droplet mean rise velocity compared with the results of Friedman and Katz (2002).	21
Figure 9	Sample PDF of droplet horizontal and vertical velocity for (a) 0.75 mm droplets and (b) 1.05 mm droplets compared with PDF of "fluid particles" and Gaussian distribution at Re_λ = 195.	22
Figure 10	Variations, with (a) St and (b) u_i'/U_q, of the droplet velocity fluctuations normalized by corresponding fluid velocity fluctuations. The estimated uncertainty is close to or smaller than the size of the symbols	23
Figure 11	Variation of normalized (a) horizontal and (b) vertical diffusion coefficients with normalized turbulence intensity.	24
Figure 12	Comparison of Lagrangian fluid diffusion time scale in horizontal and vertical directions with the rotation period of the mixer.	25
Figure 13	Variations, with u_i'/U_q, of the droplet horizontal and vertical diffusion coefficients normalized by $u_i'L_{qi}$ in (a) linear and (b) log scales.	26
Figure 14	Droplet horizontal and vertical diffusion coefficients normalized by the corresponding fluid diffusion coefficients.	27
Figure 15	Droplet horizontal and vertical diffusion time scales normalized by the corresponding fluid diffusion time scales.	27
Figure 16	(a) Diffusion coefficient of 35-70 μm oil droplets compared to fluid particle dispersion (b) Droplet diffusion coefficient scaled by the fluid diffusion coefficient as a function of u_i'/U_q including 35-70 micron oil droplets.	29
Figure 17	Sample droplet horizontal dispersion (mean square displacement) at Re_λ = 214.	30
Figure 18	A sequence of 8 images showing breakup of a crude oil droplet mixed with dispersant. The timing is indicated on each image at Re_λ=190	31

Figure 19	Snapshots of breakup of a stretched droplet at Re_λ= 214. Timing is indicated on each Figure.	32
Figure 20	Size distribution of daughter droplets for crude oil break up at Re_λ= 214.	34
Figure 21	Extension of a thread from droplet upon entering the turbulent flow region. Delay between time steps is 20 ms.	35
Figure 22	Droplets with multiple (a) two and (b) three threads extension in isotropic turbulence flow.	36
Figure 23	Formation of a droplet with a long thread extending from it, and breakup of this tail to 3 μm droplets, DOR=15. (b) Formation of an axisymmetric tail extending from the point of flow separation on the surface of the droplet, DOR=18. In both cases, crude oil mixed with dispersant is injected into quiescent fluid.	36
Figure 24	Formation of droplet with very long threads extending from them when a jet of water impinges a surface layer containing oil mixed with dispersant.	38

Table 1	Turbulence parameters during the dispersion experiments	11
Table 2	Properties of the crude oil, and changes to the surface tension due to mixing of the oil with COREXIT 9527.	12

1.0 Introduction

Efficient cleaning up of oil spills is a long-standing environmental concern. The usage of dispersants to breakdown an oil spill into droplets has generated renewed interest recently primarily due to the increasing non toxic nature of the dispersants currently being investigated, and the limitations of other available cleanup methods (Lessard and Demarco, 2000). Dispersants are water and oil soluble surfactants that lower the interfacial tension of the oil thereby accelerating the breakup the oil spill into droplets by the action of waves and oceanic turbulence. The resulting entrainment of the droplets removes the oil from the surface, and helps in mitigating its adverse effects on sea birds, mammals and subsurface life. We have been specifically interested in two aspects of this problem. The first part deals with what happens to the oil droplets formed after the oil spill is broken and how far and how fast are they transported by the oceanic turbulence. The second part involves investigation of how the oil spill breaks up into droplets, both in qualitative and quantitative sense.

Quantitative data on the dispersion rate of the droplets formed due to oceanic turbulence is needed for predicting and modeling the environmental impact of oil spills. Most of the present data on oceanic dispersion rates of fuel comes from the dye based experiments,(e.g. Talbot et al., 1974 and Morales et al., 1997), which essentially measures the dispersion rate of passive scalars rather than the buoyant oil droplets. Thus we have no field data on droplet dispersion. In looking for data in laboratory or computational studies one notes that most of the attention has been paid to transport and turbulent dispersion of bubbles or heavy particles, (e.g. Csanady, 1963, Reeks 1963, Wells and Stock, 1983, Wang and Maxey, 1993, Spelt and Biesheuvel, 1997, Poorte and Biesheuvel, 2002, Mazzitelli and Lohse, 2003, and Snyder et al., 2006). However most liquid oils have a density that only slightly deviates from that of water, more commonly being slightly buoyant. Experiments performed by Friedman and Katz (2002) show that, trends on the mean rise rate of diesel oil droplets in locally isotropic turbulence differs significantly from that of bubbles or heavy particles. Hence, data on dispersion of these slightly buoyant droplets will be helpful in further understanding the effect of an oil spill.

The main difficulty in experimental studies of particle dispersion is the need to follow their 3-D trajectories. Further complications arise from using wind tunnels that have a large mean velocity to create nearly isotropic turbulence conditions. Snyder and Lumley (1971) overcame this problem by using 10 cameras placed successively to increase their field of view. They observed that as the particle density increased, its diffusion timescale decreased and consequently its diffusion coefficient decreased. Sato and Yamamotto (1986) mounted their camera on a 3-D translation system in order to follow tracer fluid particles in real time, which inherently limited them to low Reynolds numbers. They calculated the Lagrangian autocorrelation function of the fluid particle and used it to obtain the ratio of the Lagrangian to Eulerian diffusion timescale as a function of Reynolds number. Wells and Stock (1983) measured concentration of particles originating from a fixed source. They used charged particles, whose sizes were smaller than that of the Kolmogorov scale, in an electric field as a means of varying the body force. They were thus able to isolate the effect of inertia (size) and settling velocity (which gave rise to the so-called “crossing of trajectories”). They observed that as the settling velocity increased the diffusion coefficient decreased. Poorte and Biesheuvel (2002) performed extensive measurements of dispersion of single bubbles in isotropic turbulence in a water tunnel using 3-D position sensitive detectors and observed some skewness in the PDF of bubble velocity and bubble displacement.

We have performed the measurements in a setup providing nearly isotropic turbulence with low mean fluid velocity (u_{mean}), i.e. $u'/u_{mean} \sim 8$, achieved by generating the turbulence using four symmetrically located spinning grids (Friedman and Katz, 2002). The trajectories are measured using high-speed digital holographic cinematography. To account for the finite (20%) anisotropy in the rms values of the fluid velocity in the horizontal and vertical direction we compare the diffusion of slightly buoyant droplets to those of neutrally buoyant very small particles (that could be treated as fluid particles), following the same procedure. This approach enables us to distinguish between effects of buoyancy and anisotropy.

The design of these experiments is predicated upon looking at mixing in turbulence, from a Lagrangian viewpoint, as proposed by Taylor (1921), and we utilize his theory in this report to measure the turbulent diffusion parameters. Taylor (1921) introduced a Lagrangian method for determining the diffusion rate of a scalar in stationary, homogeneous and isotropic turbulence and his theory has been and extended to particles (that do not necessarily follow the fluid) by Csanady, 1963. This theory shows that the diffusion coefficient can be calculated from the Lagrangian velocity autocorrelation function, R_{ii},

$$R_{ii}(\tau) = \int_{t=0}^{\infty} V_i(t) V_i(t+\tau) dt / V_i'^2 \qquad (1)$$

where τ is the time, $V(t)$ is the fluctuating component of fluid or particle velocity, the subscript i refers to the direction and $V_i' = (\int_{t=0}^{\infty} V_i^2(t) dt)^{0.5}$. Assuming a Fickian diffusion process, the dispersion coefficient may be estimated from

$$D_{ii}(\tau) = V_i'^2 \int_0^{\tau} R_{ii}(t') dt' \qquad (2)$$

and the mean square displacement or dispersion using

$$X_i^2(\tau) = 2V_i'^2 \int_0^{\tau}\int_0^{t} R_{ii}(t') dt' dt \qquad (3)$$

Since experimental systems are limited in the period over which the auto-correlation can be calculated, following Snyder and Lumley (1971), we obtain the diffusion coefficient of the oil droplets $D_{dii}(\tau)$ by using an ensemble average of the droplet velocity auto-covariance, i.e.

$$D_{dii}(\tau) = \int_{t=0}^{\tau} \langle U_i(t') U_i(t'+t) \rangle dt \qquad (4)$$

where U_i is the fluctuating component of the droplet velocity in direction i and <> denotes an ensemble average over all droplets of the same size and flow conditions. This approach gives us a time-dependent diffusion coefficient, which is sometimes referred to as “Quasi-Fickian”, (Deng and Cushman, 1995), and can be used in a scalar-like diffusion equation. At large τ, as the integral becomes constant, the droplet diffusion coefficient converges into the classical Fickian diffusion coefficient (D_{dii}), $D_{dii} = U_i'^2 T_{di}$, where U_i' is droplet velocity rms and T_{di} is the droplet diffusion timescale. We can use this diffusion coefficient to quantify the effect of oceanic turbulence on droplet spreading.

The second part of this report deals with the breakup of oil spill due to the addition of dispersants. Breakup of an immiscible fluid blob in another continuous fluid medium is a well studied problem in fluids literature starting from the work of Lord Rayleigh (1880), who has analyzed the instability of a cylinder of viscous liquid due to surface tension. The breakup can happen in a variety of ways depending on flow condition and fluid properties, as characterized by Hinze (1955). Subsequently, breakup of a liquid blob in a laminar flow, which can be primarily quantified by capillary number and viscosity ratio, has been widely studied and well understood as can be seen from the works of Grace (1971), Stone and Leal, (1989) and Zhang and Basaran (1995). Breakup in turbulent and high speed flows are typically characterized by the Weber number and are comparatively less understood (Eastwood, 2002). The presence of surfactants further complicates the breakup process, both by lowering surface tension and introducing the Marangoni stresses, as can be seen from Stone and Leal (1989), Janssen et al. (1997), Eggleton et al. (1999) and Jin et al. (2006). The addition of surfactants can also produce some new modes of breakup like tip streaming and tip dropping (Janssen et al., 1997), which can produce extremely small droplets. Breakup of a viscous oil spill in oceans due to the addition of dispersants happens in a turbulent environment in the presence of surfactants and hence incorporates the complexity of all the above.

2.0 Objectives

Our objectives have been:

- To measure and parameterize the effects of turbulence and oil properties on the mean settling velocity and dispersion (turbulent diffusion) rate of oil droplets.

- To obtain data on breakup of crude oil droplets and the resulting characteristic size distributions.

- To better understand the breakup process, upon addition of dispersants, and utilize the knowledge to make the process more efficient.

3.0 Methods

3.1 Facility Description

The facility shown in Figure 1, and described in detail in Friedman and Katz (2002) generates nearly isotropic turbulence with weak mean flow by using four symmetrically located rotating grids. Each grid has staggered circular hole pattern with a 40% blockage factor and slots at the top and bottom plates to reduce viscous pumping. They are attached to separate AC synchronous motors whose speed, and consequently the turbulence level, can be adjusted by variable frequency static inverters. The experiments have been performed at 225, 337.5 and 506.3 rpm's of the rotating grids. The continuous medium is de-ionized and filtered tap water and experiments are performed at a mean temperature of 20 ºC (19-21 ºC).

3.2 Turbulence Characterization

The turbulence in the central part of the tank, which extends beyond the sample volume, has been characterized using 2-D Particle Image Velocimetry (PIV) in several planes and in two perpendicular directions. The light source is an Nd:YAG laser and images are acquired using a Kodak ES 4.0, 2k x 2k digital cameras with a 105mm and 210 mm lenses for the shorter (x-y) and longer (y-z) side, respectively. The delay between exposures varies between 2.5-4 ms, depending on turbulence intensity. Hollow glass beads with 7-10 μm diameter are used as tracers. The digital images are enhanced using modified histogram equalization and the velocity

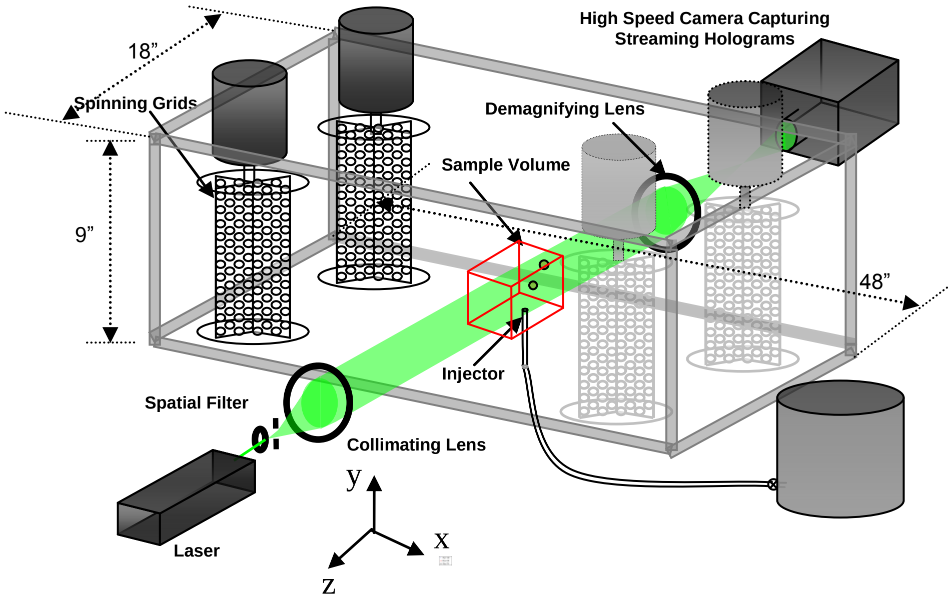

Figure 1: Turbulence generating facility with the optical setup of one view digital holography.

vectors are determined using cross correlation analysis (Roth and Katz, 2001). With 50% overlap between neighboring windows, the number of vectors in a PIV plane varies from 62x62 to 40x40 and, based on magnification, the vector spacing varies from 0.9mm to 1.7mm. At least 1000 vector maps are averaged for each condition to obtain the turbulent statistics, and consequently the associated uncertainty is at least an order of magnitude smaller than the measured parameters. Measured turbulence parameters for the three mixer speeds are provided in Table 1. The energy spectra have a slope close to -5/3and since the spatial resolution of the PIV data is not fine enough to estimate the dissipation rate, it is estimated by fitting -5/3 slope lines to the inertial part of the kinetic energy spectra. The turbulence scales are subsequently calculated using

$$\eta=\left[\nu^3/\varepsilon\right]^{0.25},\ \tau_\eta=\left[\nu/\varepsilon\right]^{0.5},\ L=\left[u'^3/\varepsilon\right] \text{ and } \lambda=u'\left[15\nu/\varepsilon\right]^{0.5} \qquad (5)$$

where η is the Kolmogorov length scale, ν is viscosity, ε is dissipation rate, τ_η is the Kolmogorov time scale, L is the integral length scale and λ is the Taylor microscale. Statistics for the present three turbulence levels calculated using the above equations are also provided in Table 1. The 20-25 % anisotropy is characterized by the ratio of the spatially averaged rms velocity. Given these results, in the rest of the report we assume that the turbulence in the facility is homogeneous, stationary and nearly isotropic. As noted before the effects of anisotropy are accounted for in the analysis.

3.3 Sample Preparation and Characterization

For the dispersion part of the experiments the oil used is research grade diesel fuel (LSRD-4) with specific gravity of 0.85, provided by Specified Fuels and Chemicals of Channel-view Texas. The oil is injected from 0.15 mm diameter needles directly into the facility, near its central region. The property of this oil does not vary significantly with time or sample, making it ideal for dispersion experiments, where we are more interested in transport properties of turbulence rather than oil characteristics.

Mixer rpm	225	337.5	506.3
Vertical Mean Velocity, $u_{y\ mean}$ (cm/s)	0.56	0.78	1.02
RMS Velocity, u' (cm/s) $u' = \sqrt{(u_x'^2 + u_y'^2 + u_z'^2)/3}$	4.63	7.1	9.4
Anisotropy ratio, u_y'/u_x'	1.24	1.26	1.2
Dissipation, ε(m^2/s^3)	0.0019	0.0099	0.0256
Integral Length Scale, L (mm)	52	35	32
Integral time scale, $T_f = L/u'$ (s)	1.12	0.49	0.34
Kolmogorov Length Scale, η(mm)	0.151	0.1	0.079
Kolmogorov Time Scale, τ_η (s)	0.0229	0.01	0.0063
Taylor Micro scale,λ(mm)	4.11	2.75	2.28
Taylor Scale Reynolds Number, $\mathrm{Re}_\lambda = u'\lambda/\nu$	190	195	214

Table 1: Turbulence parameters during the dispersion experiments

For the breakup part of the experiments, the sample crude oil has been collected from the Alaska National Slope with minimum additives and provided by OHMSETT. The dispersant used is COREXIT 9527, obtained *gratis* from Nalco/Exxon Energy Chemicals, one of the most predominantly stockpiled dispersants in United States.

During the breakup tests, 10 ml of the crude oil is mixed with 0.5 - 0.66 ± 0.02 ml of dispersant (i.e. dispersant to oil ratio (DOR) of 1:20 to 1:15) in a small container and they are mixed by vigorous shaking, followed by quiescent diffusion, before the well mixed sample is injected into the turbulent facility by a 0.15 mm ID hypodermic needle. The volatility and variability in the properties of crude oil along with the dependence of the breakup process on oil properties makes it essential to carefully measure the properties of the oil that we use.

Specific Gravity is measured by measuring the extra weight due to the addition of 75 ml of the crude oil. The Viscosity is measured using Canon glass capillary viscometer. Two Viscometers with different ratings are used, and the difference between their readings and the difference between multiple readings from the same viscometer are used to determine the uncertainty of the measurement. The surface tension is measured by measuring the height difference (hydrostatic pressure difference), as shown in Figure 2, required to transform a flat surface into and hemisphere. The surface tension coefficient is obtained, for DOR of upto 1:20, using the Laplace equation. For higher DOR, the surface tension is estimated from the oblateness and quiescent rise rate of the droplet (U_q), following Hu et al (2000). Measured properties of the crude oil used in our experiments are presented in Table 2.

	Specific Gravity	Kinematic Viscosity (mm^2/s)	Surface Tension (mN/m)
Crude Oil	0.847	7.1 ± 0.08	16.7
DOR 1:20	0.851	8.99	0.69
DOR 1:18.2	0.852	9.25	0.63
DOR 1:15.2	0.853	9.60	0.16

Table 2: Properties of the crude oil, and changes to the surface tension due to mixing of the oil with COREXIT 9527.

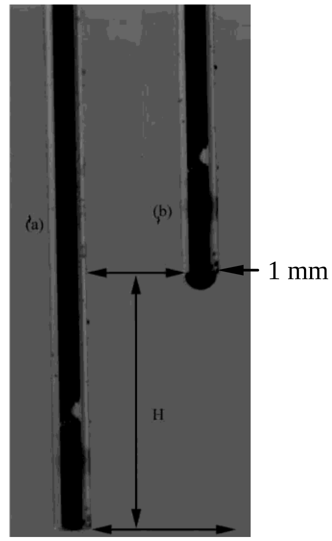

Figure 2: Surface tension measurement using capillary tubes.

3.4 Droplets and Fluid Dispersion Measurements

Our objectives require measurements of the time history of a target moving in a “random” 3-D trajectory over scales that exceed the integral scale of turbulence. We would also like to measure the droplet size accurately to better characterize the dispersion process. Holographic particle image velocimetry is particularly suited for measuring the instantaneous 3-D location, shape, size and velocity of many particles located in a sample volume with an extended depth, e.g. Meng and Hussain (1991), Tao et al. (2002), Sheng et al. (2003). In the present study we use inline digital holography using setup illustrated in Figure 1. Here, the same beam is used for illuminating the particles and as a reference beam, simplifying the optical setup. Forward scattering from particles greatly reduces the power requirement of the laser, by more than 3 orders of magnitude, allowing high speed imaging with a relatively low cost laser. The part of the beam, which is not scattered by the particles, acts as a reference beam as long as the particle concentration is low.

Figure 1 shows the optical setup for recording a single view in-line hologram. A 0.1 mj/pulse, 523 nm (green), Nd:YLF laser beam passes through a spatial filter, which improves the beam profile, and a collimating lens before illuminating the 50x50x70 mm^3 sample volume in the center of the tank. The beam is then de-magnified by 2.9:1 and recorded by the high speed camera at a resolution of 1k x 1k (pixel size 17 μm), and at speeds ranging between 250 to 1000 frames/sec, depending on the mixer rpm. At the present magnification, the lateral resolution is around 50 μm/pixel. To maintain a uniform background, the recorded hologram is divided by a background image obtained by averaging thousands of images. The digital holograms are reconstructed numerically for a specified distance in the beam axis direction, using the Fresnel approximation, which involves convolution of the intensity distribution with a far-field source function. Details of the procedure are available in Milgram and Li (2002), Malkiel et al. (2003) and in Sheng et al. (2006).Reconstruction is repeated every 2 mm and consequently each instantaneous 3-D image consists of 35 planes. The spacing of the reconstruction plane is governed by the so called depth of focus problem, namely that the location of the particle in the beam axis direction is less accurate than the lateral resolution. We initially recorded 2 perpendicular hologram, following Tao et al. (2002) and Malkiel et al. (2003), in order to obtain accurate 3-D tracks. Later we have shifted to a single view since we only need to resolve the dispersion in vertical and one horizontal direction. Consequently the measurement provides data on velocity time series in two directions x and y.

We have also obtained Lagrangian database for the trajectories of neutral density (specific gravity~1.03), 50 μm diameter Polyamide particles, which we treat as Lagrangian fluid tracers, in order to completely account for the effect of turbulence anisotropy. This Lagrangian fluid data is also obtained using one view in-line holography, using an experimental setup that is identical to that used for obtaining the droplet tracks. The dilute particle solution is introduced into the sample volume at a very low velocity. During these experiments, an extra filtering loop is added to the facility with a 25 μm filter to further filter the de-ionized water between subsequent data acquisitions to minimize the impurities in the water, and reduce the noise in the recorded holograms.

Further experiments have been performed to observe diffusion of very small oil droplets, with size varying from 35-70 μm. These small oil droplets are produced by adding dispersant COREXIT 9527 to the crude oil and using a magnetic stirrer to mix it with water. The resulting dilute solution of oil in water is injected, similar to the Polyamide particles. Preliminary investigations with microscopic digital holography have confirmed that this procedure effectively achieves reproducible droplet sizes, if we keep the container at rest for 5 minutes after stirring and before injection. In order to observe droplets of size ~ 35-70 μm, we have to reduce the field of view to 34x34x70 mm^3, i.e. increase the magnification. This phase of the project has not been completed when the CRRC grant expired, and at the present time we only have preliminary data.

3.5 Tracking of Oil Droplets and Fluid Particles

Hybrid Labview and C++ based processing software has been developed for an automated analysis of the holograms in order to obtain the droplet tracks. The software is divided into two parts. The first part measures the location of the droplets as well as their size, and the second part matches the traces of the same droplet in successive frames, which provides the droplet velocity. The droplets in the reconstructed holograms have pixel values in the range of 25-75 (out of a total range of 0-255) irrespective of their spatial (x-y) or beam (z) axis location. Hence a double threshold between 25-75 is applied on the reconstructed hologram, which reduces it to a binary image for further segmentation. Since we do not observe significant deformation of the droplet from a spherical shape, we use the circularity filter of the Labview software which performs segmentation of the binary image and gives us the location and size of the droplets. An additional advantage is that the circularity filter can recognize overlapping droplets to a certain degree, making the droplet tracking more efficient. The circularity filter of Labview assumes that all objects in the field of view are circles. Hence, if a blob formed as a result of overlapping droplets does not satisfy the circularity conditions, the filter tries to fit two or more circles into the blob. As long as the droplets are only partially overlapped, this filter correctly predicts the spatial location of overlapping droplets.

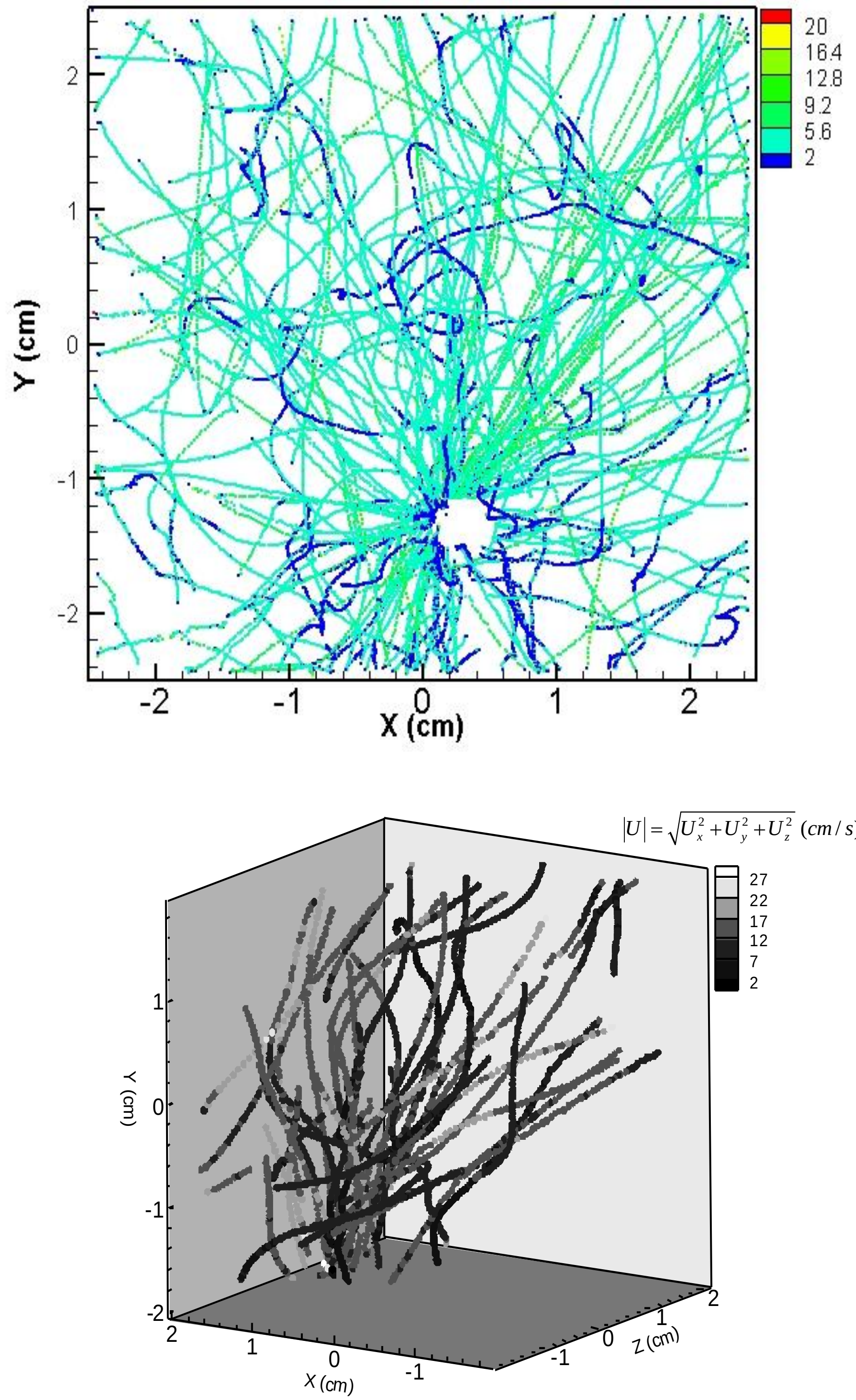

(b)

Figure 3: A sample (a) 2-D projection and (b) 3-D matched droplet tracks with grayscale showing velocity magnitude.

With the droplet parameters obtained, we match the traces of the droplets in successive frames by using the following criteria:

1) Closest point in the next time step.
2) Radius within a certain tolerance range.
3) Depth within a certain tolerance range.
4) Limitation on maximum acceleration.
5) Avoiding sharp jitter (sudden change in acceleration).
6) Extrapolation of tracks based on previous slopes to find subsequent images in cases where the droplets at different depths cross each other.

In order to obtain 3-D tracks (for the data sets that have two views) we perform the steps mentioned before for each of the two perpendicular views and then match the 2-D projection of tracks by using least squared difference in the common vertical direction. Figure 3 a and b show sample 2-D projection of 3-D droplet tracks and 3-D droplet tracks at Re_λ = 190, with the shading indicating the magnitude of the velocity. Since the shape and size of the droplet does not change appreciably in time, cross correlation of the in-focus droplet images is used to obtain the droplet velocity. We first apply a 3x3 Sobel high pass filter on the droplet image so that only the edges are cross correlated.

As we also know the droplet velocity approximately, from the subtraction of the droplet displacement, to maintain accurate measurement of droplet velocity, we vary the time gaps between images used in cross correlation to ensure sufficient displacement between the droplet locations. Our criterion maintains the uncertainty of the droplet velocity to be at most 25% of the Kolmogorov velocity (η/τ_η, about 1 cm/s), not taking into account the extra accuracy gained by high pass filtering of the images. The local mean fluid velocity, which is measured using PIV, is subtracted from each instantaneous droplet velocity to obtain the droplet velocity in the absence of the mean fluid flow. The difference in the diffusion coefficient obtained by subtracting the local mean fluid velocity in comparison to no fluid velocity subtraction is less than 2%, i.e. it has little effect on the result, showing that the effect of local mean fluid flow on the droplet dispersion is negligible.

When tracking fluid particles and 35-70 μm oil droplets we have to modify the software used for obtaining their spatial location, since the small size makes the circularity filter unfit for identification. The algorithm has been initially developed for the polystyrene particles but later used for the 35-70 μm oil droplets with no changes. The analysis involves growing the particle images to a bigger size (as the segmentation routines do not pick up very small particles), thresholding to identify particle centers, and application of a low pass filter and a second threshold to produce a binary image of the enlarged particle. A particle detection routine in Labview is then used to obtain the spatial coordinates of the particles from the binary images. The matching of particle traces between subsequent frames is performed following the procedures adopted for droplets. We have performed extensive manual checking by observing reconstructed movies of the tracked data, to confirm its accuracy in picking up particles and tracking them. The accuracy of the tracks is confirmed independently by the fact that the maximum deviation between measured fluid velocity rms (Lagrangian) and the mean rms value obtained from PIV measurements (Eulerian) is ~ 6%. Since the sub-pixel curve fitting is not useful for the very small 1-4 pixel particles, the accuracy in measuring fluid particle displacement is conservatively estimated ~0.5 pixels. We again maintain the uncertainty of the fluid particle velocity below 33% of the Kolmogorov velocity by varying the time gap.

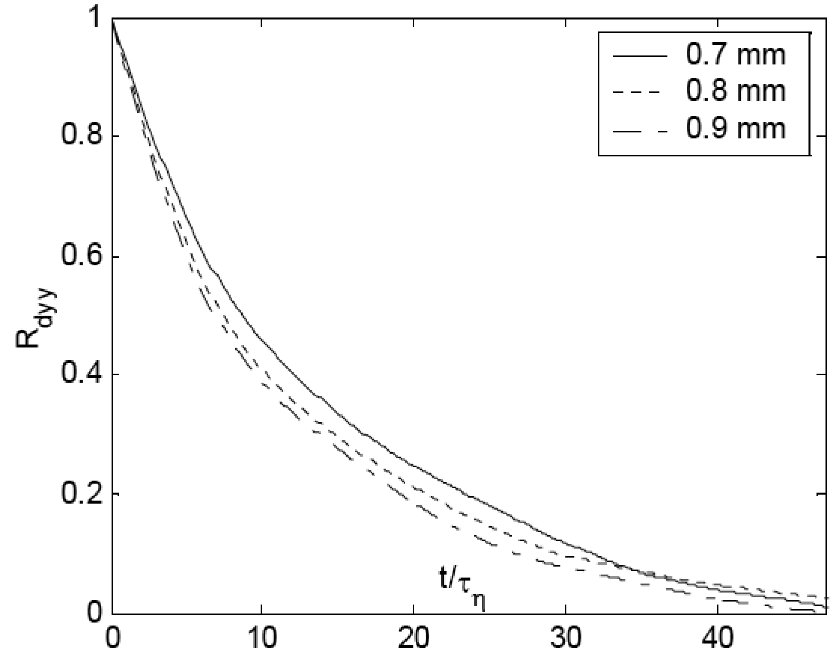

Figure 4: Sample ensemble averaged droplet Lagrangian velocity autocorrelations at Re_λ = 214.

Using the above mentioned procedures we have obtained the velocity time series of more than 17,000 droplets in one view and 4000 droplets in two views, ranging in size between 600 and 1200 μm. Also, 15000 neutral density particles and more than 1500, 35-70 μm, oil droplet tracks have been obtained. As noted above, the task of tracking very small droplets and calculating their diffusion has not been completed.

3.6 Calculation of Diffusion Parameters

Analysis of oil droplet dispersion is based on the one-view measurements. During analysis, the droplets are binned based on size in steps of 100 μm consistent with our spatial resolution. Thus, the entire database is split into seven bins. While analyzing the droplet dispersion variation with size, we use a 3-bin running average in order to increase the number of droplets per bin, while giving the central bin twice the weightage. Hence the data of droplet dispersion coefficient is presented for 5 different sizes in the 700-1100 μm size range for Re_λ = 190 and 195, and for 3 different sizes, in the 700-900 μm range for Re_λ = 214 (due to insufficient droplets in the last two bins). For different droplet sizes, the Reynolds number, based on the droplet diameter and droplet quiescent rise velocity, varies from 14 to 37.

Sample ensemble-averaged droplet autocorrelation functions, $R_{dii}(\tau) = \langle U_i(t)U_i(t+\tau)\rangle / U_i'^2$, extending to time scales for which the diffusion becomes almost Fickian, i.e. the autocorrelation decreases to zero, are presented in Figure 4. Figure 5 shows the variation with time of the horizontal droplet diffusion coefficients, $D_{dxx}(t)$,for different droplet sizes, and the corresponding horizontal fluid particle diffusion coefficient, $D_{fxx}(t)$, calculated using equation 4, for Re_λ = 190 and 214. In calculating the Lagrangian fluid velocity data, we replace the droplet velocity by the "fluid particle" velocity. The asymptotic value of $D_{fxx}(t)$ provides the Fickian fluid diffusion coefficient, D_{fii} .In some cases $D_{dxx}(t)$ (or $D_{fxx}(t)$) does not reach a plateau, since the tracks are not sufficiently long to reach convergence to a fixed Fickian value. For these cases (only), to estimate the Fickian diffusion coefficient, we use a lowest order (4-6) polynomial fit to extrapolate the available data to a plateau. In evaluating the accuracy of this extrapolation method, using cases for which we have a converged value, we find that the maximum uncertainty in the extrapolated Fickian diffusion coefficient is about 6%. Also, in some cases, the auto-correlation function decreases to small negative values (not shown), which would cause a slight decrease of $D_{dii}(t)$ beyond its maximum value. In these cases, we use the maximum value for the diffusion coefficient to prevent the finite size of the field of view, which might induce negative correlations, from biasing the data towards lower values.

We have also performed a "Bootstrap uncertainty analysis" for the droplet diffusion coefficient by taking a random sample of 67% of the droplets in a bin and re-calculating the diffusion coefficient. The uncertainties of the sub-samples are estimated by repeating this process for 250 realizations for each of the bins. Based on the ratio of twice the rms of the variations of the diffusion coefficient to the mean value, the uncertainty is in the range of 3-6%. It is included as error bars in Figure 13 a.

3.7 Dimensional Analysis of Dispersion Coefficient

Following Spelt and Biesheuvel (1997) and Friedman and Katz (2002), scaling of the Fickian diffusion coefficient of droplets in turbulent flows can have the following dependence

$$D_{ii} = f(u_i, \rho_c, \rho_d, \mu_c, L, d, g) \qquad (6)$$

The droplet viscosity is not included, since the "unclean" water causes the droplet to behave like a solid sphere (Friedman and Katz, 2002). Also, the spherical shape of the droplets indicates that interfacial tension is not a dominant parameter, which is not the case when dispersants are added, as discussed later. Non-dimensionalizing, and introducing the quiescent rise rate of droplets, U_q, and its characteristic response time scale, τ_d, instead of density ratio and droplet diameter, one obtains

$$D_{dii} / Lu_i' \text{ or } D_{dii} / LU_q = f(u_i'/U_q, Re_\lambda, St) \qquad (7)$$

where L is the turbulence integral length scale and u_i' is the fluid velocity rms. The turbulence level is characterized by the Taylor micro-scale Reynolds number, $Re_\lambda = u'\lambda/\nu$, where $u' = \sqrt{(u_x'^2 + u_y'^2 + u_z'^2)/3}$, λ is the Taylor micro-scale and ν is the kinematic viscosity. The effect of droplet properties are accounted for in part by the Stokes number (St), which is defined as $St = \tau_d / \tau_\eta$, where τ_d is the droplet response time and τ_η is the Kolmogorov time scale. The response time of the droplet is calculated using a Stokes flow assumption, giving $\tau_d = \rho_d d^2 / 18\mu_c$ (section 2.3 of Crowe et al., 1998), where ρ_d is the droplet density, d is the droplet diameter and μ_c is the dynamic viscosity of the fluid. Droplet properties are also affected by u_i'/U_q, where U_q is the quiescent rise velocity of the droplets, which is obtained following Friedman and Katz (2002). They have estimated U_q by treating the droplets as rigid particles and equating the net buoyant force with the drag force, and then confirmed it by measurements, especially for larger droplets. This functional relationship is also applicable for the droplet mean rise velocity and droplet velocity fluctuations, which are scaled by the droplet quiescent rise

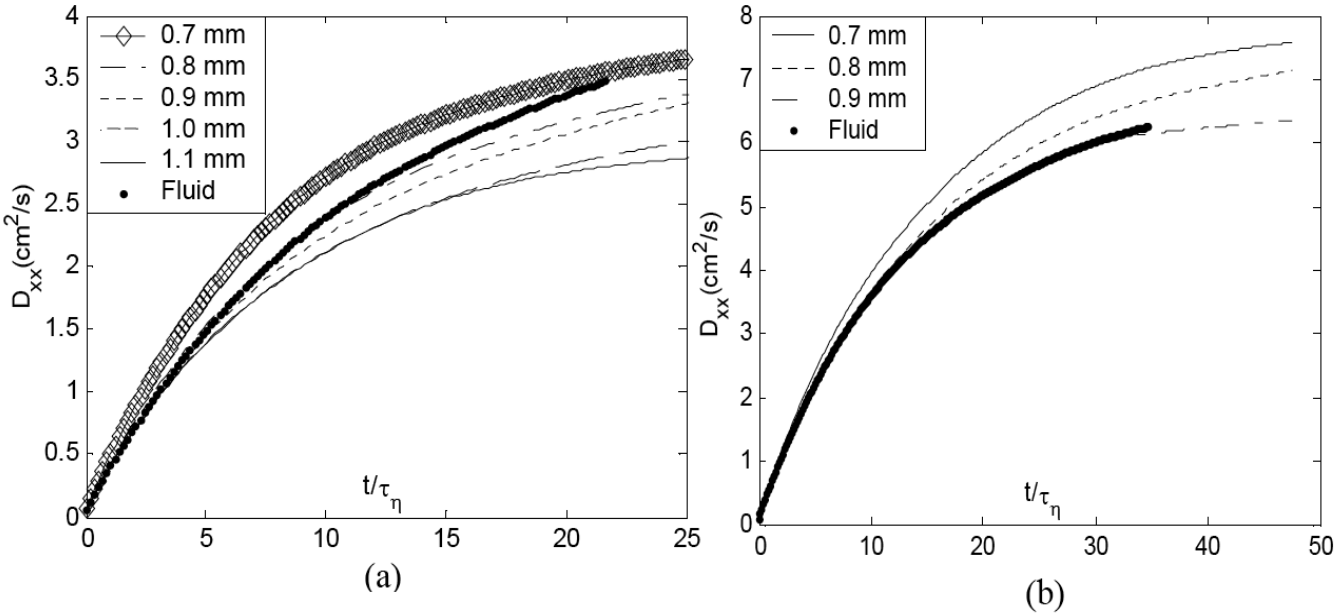

Figure 5: Fluid and droplet (different sizes) horizontal diffusion coefficient as a function of time for (a) Re_λ = 190 (low u_i'/U_q) and (b) Re_λ = 214 (high u_i'/U_q)

velocity and fluid velocity fluctuations respectively. As we show later, u_i'/U_q is the dominant scaling parameter for the current droplet sizes and turbulent intensities.

3.8 Droplet Breakup Visualization

The same facility (Figure 1) is used for the droplet dispersion experiments. These experiments are performed at 225 and 506.3 rpm's of the rotating grids. The sample crude oil from Alaska National Slope is mixed with the dispersant COREXIT 9527 and is injected using 0.15 mm diameter needles by manual pressure injection. The needle is enclosed in a small cylindrical container to damp the flow near the point of injection to minimize effects occurring as the droplet separates from the needle. The droplets formed in near quiescent conditions rises up due to buoyancy and are entrained by the turbulent flow. The continuous medium is de-ionized tap water and experiments are performed at a mean temperature of 20 ºC (19-21 ºC). The visualization setup is similar to the one illustrated in Figure 1, with the only variation being the usage of 105 mm Nikon lens instead of the de-magnifier, hence the resulting field of view decreases to 17x17x70 mm^3.

3.9 Visualization of Droplets in Quiescent Flow and Impinged Surface

We have also examined the behavior of droplets treated with dispersants during injection into a quiescent fluid. The test facility is a 25.4x25.4x101.6 mm^3 container with a hole in the bottom for inserting the hypodermic needle. The droplet injection and rise in quiescent conditions are visualized using both digital inline holography, i.e. the same procedures that are those used during the turbulence measurements, or white light, high speed image acquisition, as illustrated in Figure 6. Here, we have used different lenses from telescopic to microscopic in order to

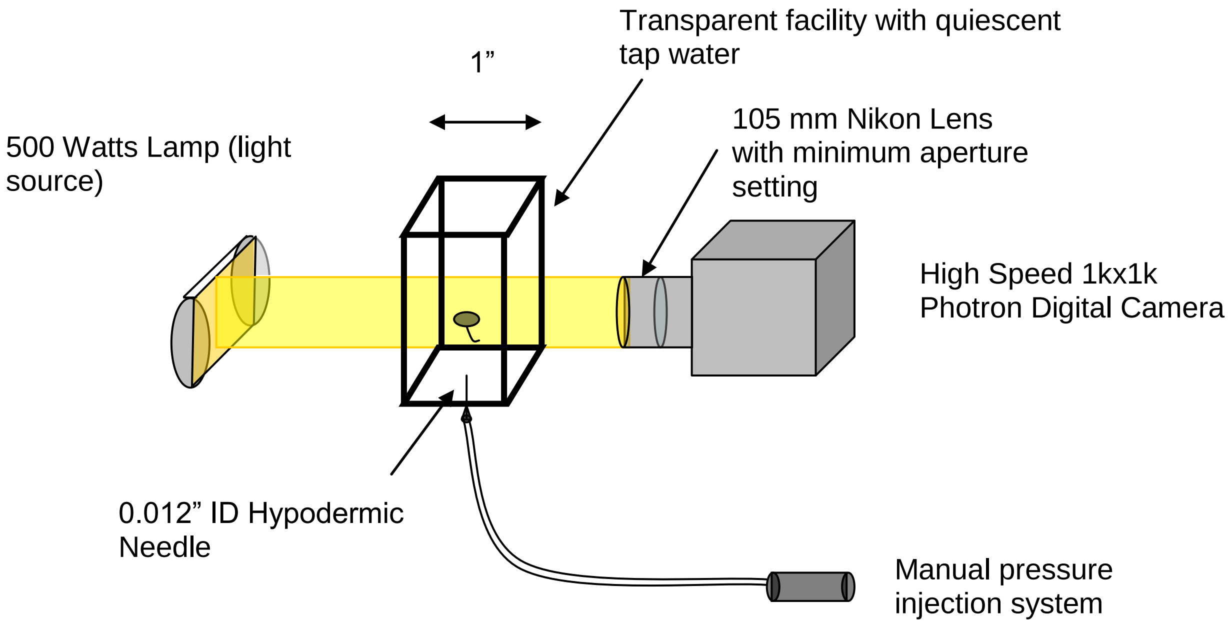

Figure 6: Visualization experiments in quiescent flow.

observe the phenomenon in different magnifications. Droplet injection experiments were performed for DOR varying from 1:20 to 1:12.

To examine the breakup of an oil droplet treated with dispersant located on the surface, we use the same small container. The oil that is premixed with the dispersant is spilled delicately at the water surface, similar to usual wave tank experiments. After the system becomes quiescent, drops of liquid water are impinged on this oil spill and the effect is visualized using the high speed imaging system, similar to that shown in Figure 6.

4.0 Results

4.1 Transport of Diesel Oil Droplets

This section deals with the analysis of the diesel oil time series data. In particular, we look at the PDF of velocity, mean rise velocity, rms of velocity and diffusion coefficient of droplets. As explained in the introduction, these quantities describe statistically all the information that could be extracted from observing the spreading of oil droplets in dilute concentration. Also, as we can see clearly from the result, the dynamic behavior of droplets primarily depends on the parameter u_i'/U_q, where u_i' is the rms value of liquid velocity fluctuations, and U_q is the rise rate of the droplets in quiescent water. Hence the data that we obtain from the diesel oil droplets can be used for most crude oils, most of which have density that is close to that of the diesel oil. These conclusion should be verified in experiments involving crude oil droplets of varying density.

4.1.1 Mean Rise Velocity

From the Lagrangian droplet velocity time series data, we first obtain the mean droplet velocity for each size bin after subtracting the mean fluid velocity, as mentioned before. The horizontal mean droplet velocity components are an order of magnitude smaller than the vertical components and are present only due to the finite data size and slight inhomogenity in the flow. The difference between droplet mean rise velocity (U_{slip}) and the droplet quiescent rise velocity normalized by the droplet quiescent rise velocity is shown in Figure 7. Results are plotted against the Stokes number, which is commonly used as a parameter for characterizing behavior of particles in turbulent flows. Clearly, this type of scaling does not collapse the data onto a meaningful curve. Figure 8 compares the current data with that of Friedman and Katz (2002) using their scaling. In this case, all of our results do collapse onto a single curve, confirming that their scaling is correct. In agreement with their results, which have been obtained in part in the same facility (except for the highest u_i'/U_q), we observe that for $u_i'/U_q > 3.5$ the mean rise velocity is enhanced by turbulence regardless of Stokes number, and significantly exceeds the rise rate of droplets in quiescent fluid. Also, at a given Stokes number, the droplet's rise velocity increases with turbulence level (Figure 7), from values that can be lower than U_q to levels that are much higher than the quiescent rise rate. As explained in detail in Friedman and Katz (2002), this enhancement is most probably due to trajectory biasing, i.e. rising droplets are preferably swept towards the upward flowing region of turbulent eddies.

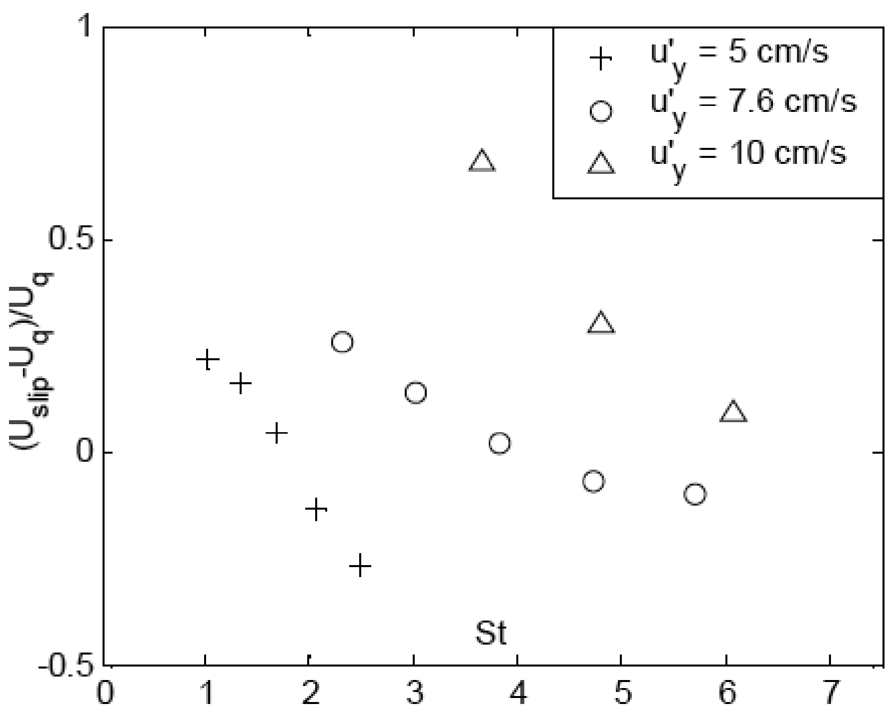

Figure 7: Droplet mean rise velocity normalized by the quiescent rise velocity as a function of Stokes number. The corresponding Re_λ are 190, 195 and 214.

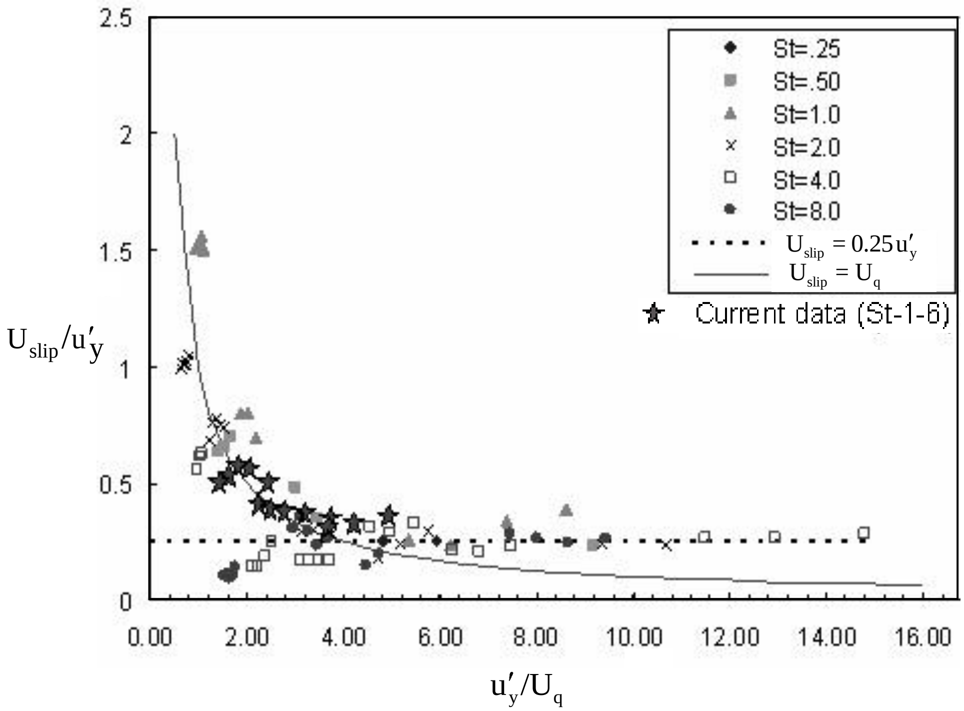

Figure 8: Droplet mean rise velocity compared with the results of Friedman and Katz (2002).

4.1.2 PDF of Velocity Fluctuations

To obtain the time history of the droplet and neutrally buoyant particle velocity fluctuations, we subtract the mean velocity from the instantaneous values. For the purpose of obtaining the probability density function (PDF) of the droplet velocity fluctuations, with a sufficiently large database (to obtain converged statistics), the data at each turbulence level is separated into two bins, with mean sizes of 0.75 and 1.05 mm. Sample results, shown in Figure 9 a and b for Re_λ = 195, confirm that all the distributions are close to Gaussian. A nearly Gaussian distribution is essential for the present analysis because it implies that the PDF of the droplet displacement in any time step is also Gaussian (Batchelor, 1950). Indeed PDF's of droplet displacement over periods that are an order of magnitude higher(not shown), compared to the period used to obtain the droplet velocity, also have a Gaussian distribution. A Gaussian process, i.e. a time varying random process where the distribution at any instance is Gaussian, can be completely determined by a mean, a variance and an autocorrelation function (Pope, 2000). Hence, applying Taylor's (1921) analysis should provide us with statistically complete information on the dispersion of droplets.

4.1.3 Droplet Velocity Rms

We find that examining the variations of rms of droplet velocity fluctuations, U_i', as a function of u_i'/U_q, instead of Stokes number (*St*) that is traditionally used, provides a clear trend, as can be seen from Figure 10 a and b. Hence the variations of droplet velocity rms are analyzed in this

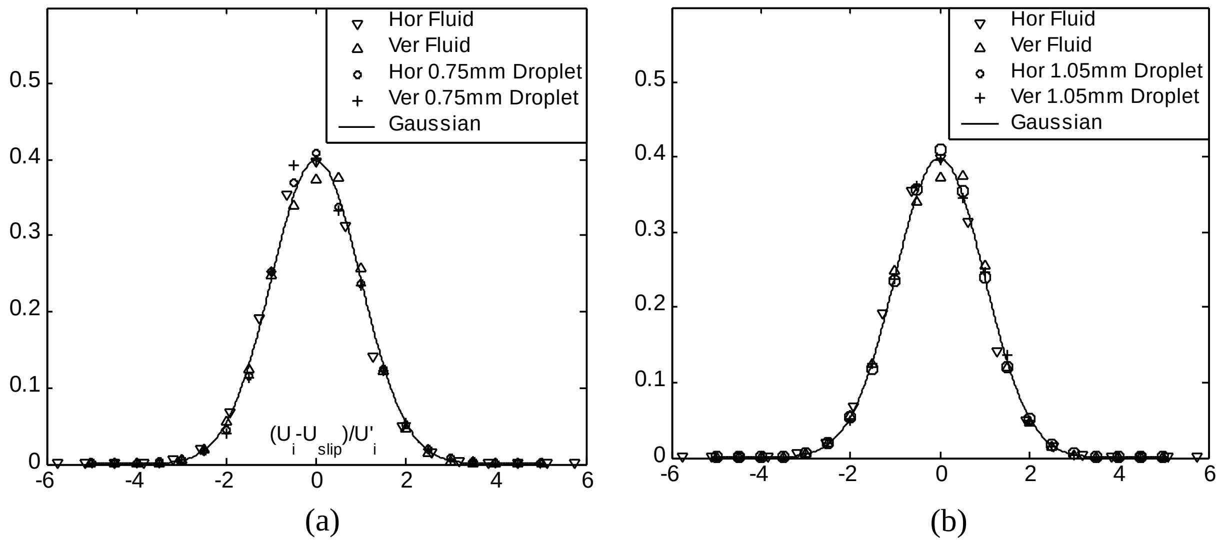

Figure 9: Sample PDF of droplet horizontal and vertical velocity for (a) 0.75 mm droplets and (b) 1.05 mm droplets compared with PDF of "fluid particles" and Gaussian distribution at Re_λ = 195.

section as a function of u_i'/U_q.In the horizontal direction, data from all measurements, i.e. different droplet sizes and turbulence levels, appear to collapse onto a single curve in Figure 10b, showing that U_x'/u_x' increases with increasing u_x'/U_q. In the vertical direction, the data do not collapse as well as in the horizontal direction, but the trend of increasing U_y'/u_y' with increasing u_y'/U_q still persists. Though the variations of the scaled droplet velocity fluctuations with u_i'/U_q are small compared to the mean value, 15-20% over the entire span of data, these variations are still substantially larger than the error bound (1-2.5%), which in all cases is smaller than or close to the size of the symbols. Note also that as the droplet diameter *(d)* becomes very small, well below the present range, one should expect that the scaled rms values of the droplet velocity approach unity, which we have observed for the 35-70 micron oil droplet experiments (discussed later). Thus, the present trends cannot persist for very large u_i'/U_q or very small *St*. These trends include the rms of the droplet horizontal velocity fluctuations exceeding those of the fluid and the droplet vertical velocity fluctuations being higher than those of the fluid only for the highest turbulence level, but lower in the other two cases. Rms values of velocity fluctuations of a dispersed phase exceeding those of the continuous phase have been observed before only for bubbles, experimentally by Poorte, (1998) and Colin and Legendre (2001) and numerically by Spelt and Biesheuvel (1997, 1998). Also, clearly the scaled horizontal droplet velocity fluctuations are higher than the vertical values, but the difference decreases with increasing u_i'/U_q.

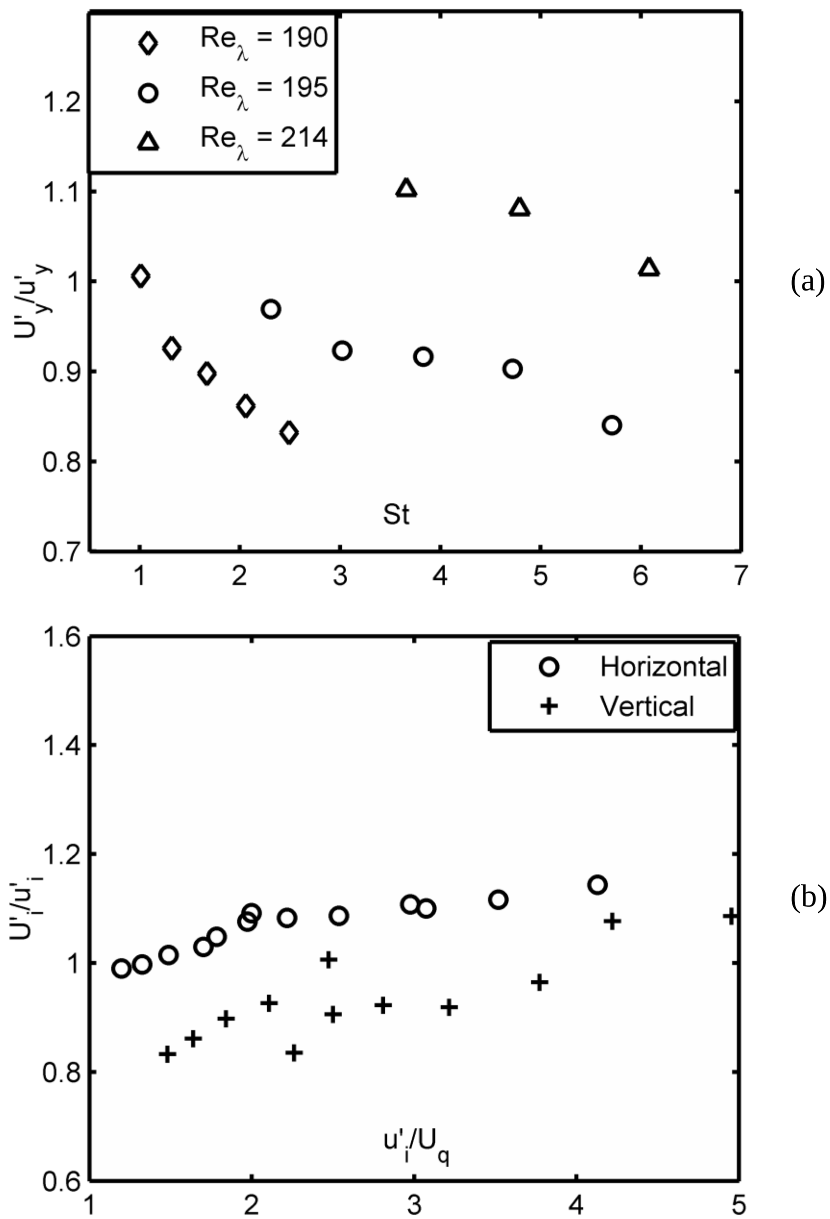

Figure 10: Variations, with (a) St and (b) u_i'/U_q, of the droplet velocity fluctuations normalized by corresponding fluid velocity fluctuations.

4.1.4 Scaling of Droplet Diffusion Coefficient

As we are interested in the application of the current data for oceanic oil spill modeling, where the length scales are much larger than the laboratory length scales, we have tried to scale the droplet diffusion coefficients with several measured Eulerian and Lagrangian turbulence parameters. After numerous attempts, we have identified scaling parameters that encompass all our data. Figure 11 shows that for all Reynolds numbers, directions and sizes (*St*), the asymptotic droplet diffusion coefficient scaled by the product of the turbulent intensity and turbulence integral length scale, monotonically increases as a function of u'/U_q.

$$D_{dii} / u'L = f(u' / U_q) \quad (8)$$

This formulation uses u' and L for both directions, i.e. we assume that the turbulence is isotropic. If we use turbulence parameters aligned in the same direction, i.e. u'_i / U_q and $L_i = u_i'^3 / \varepsilon$, the data becomes more scattered in the horizontal direction, suggesting that Eulerian directional scaling is not appropriate.

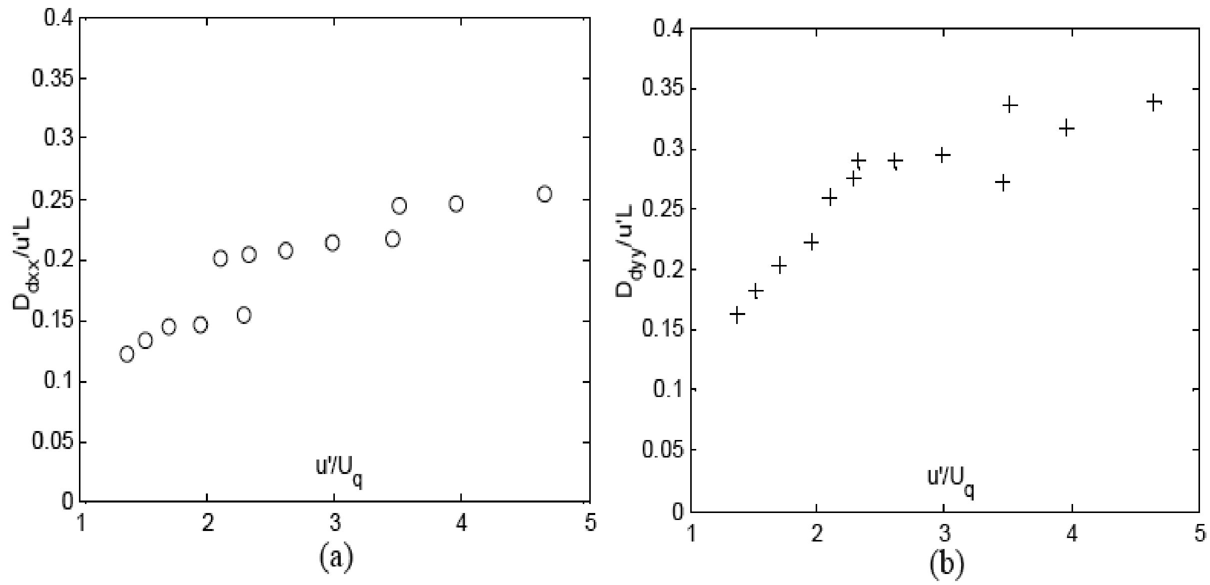

Figure 11: Variation of normalized (a) horizontal and (b) vertical diffusion coefficients with normalized turbulence intensity.

This trend is elucidated when we examine the fluid diffusion time scale, i.e. the fluid diffusion coefficient D_{fii} divided by the mean squared fluid velocity, $T_{fi} = D_{fii} / u_i'^2$, in Figure 12. Clearly T_{fx} and T_{fy} are almost equal to each other and are consistently very close but slightly lower than the period of our mixers. The method that we use to artificially force the turbulence to remain stationary, by the action of the mixers, influences the turbulent diffusion timescale (Mordant et al., 2001). Using this timescale, we can define new length scales $L_{fi} = u'_i T_{fi}$ or $L_{qi} = U_q T_{fi}$, which accounts for the Lagrangian nature of dispersion and hence the artificial forcing, that would be more appropriate than the Eulerian eddy size (L). Before proceeding, the Eulerian directional scaling and the Eulerian isotropic scaling of the droplet diffusion coefficient do not differ much for the vertical direction due to the fact that the variation in anisotropy (u'_y / u'_x) for the three Reynolds numbers is due to the horizontal rms, i.e. u'_y / u' ($u' = [(u_x'^2 + u_y'^2 + u_z'^2)/3]^{0.5}$), and hence L_y / L are constant for the three Reynolds numbers. Also, the Eulerian isotropic scaling of the droplet diffusion coefficient works better than the directional scaling for the horizontal direction because the deviations of L / L_{fx} are smaller than those of L_x / L_{fx}.

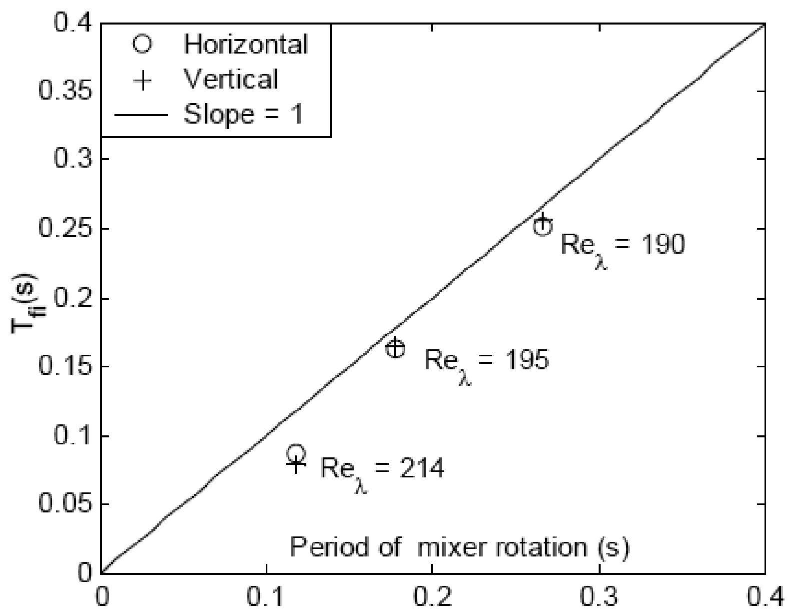

Figure 12: Comparison of Lagrangian fluid diffusion time scale in horizontal and vertical directions with the rotation period of the mixer.

When we scale the droplet diffusion coefficient using u' and the two new length scales, as shown for $D_{dii}/u'L_{qi}$ in Figure 13, in linear and log scales, we observe a similar collapse of the entire data onto a single curve, suggesting that

$$D_{dii}/u'L_{fi} = f(u'_i/U_q) \text{ or } D_{dii}/u'L_{qi} = f(u'_i/U_q) \tag{9}$$

The former relation is equivalent to scaling the droplet diffusion coefficient by the fluid diffusion coefficient and treated in detail in the next section. Also, as mentioned in Section III, error bars for the droplet diffusion coefficient estimated using "Bootstrap uncertainty analysis" are shown in Figure 13a. In data points for which the error bars are not shown, the uncertainty is less than the symbol size. To facilitate the application of this data for oceanic modeling purposes, we tried to fit a curve to our data. A straight line fit to the log plot, i.e. a power law with an exponent of 1.44 for the horizontal direction and 1.52 for the vertical direction seems appropriate. For the present range of St and u'_i/U_q, the empirical equation for the droplet horizontal and vertical diffusion coefficients are

$$D_{dxx}/u_x'^2T_{fx} = 0.66(u'_x/U_q)^{0.44} \quad \text{and} \quad D_{dyy}/u_y'^2T_{fy} = 0.51(u'_y/U_q)^{0.52} \tag{10}$$

The standard deviation of the data from this relation is 0.034 and 0.069 for the horizontal and the vertical directions, respectively. This power law behavior implies that the functional relationship using L_{fi} and L_{qi} are identical. Note that this equation is not valid in the limit of $u'_i/U_q >> 1$, where one would expect that $D_{dii} = u_i'^2T_{fi}$. This issue should be further investigated by measuring the diffusion of very small droplets, as we have started doing. Also, under the opposite limit of

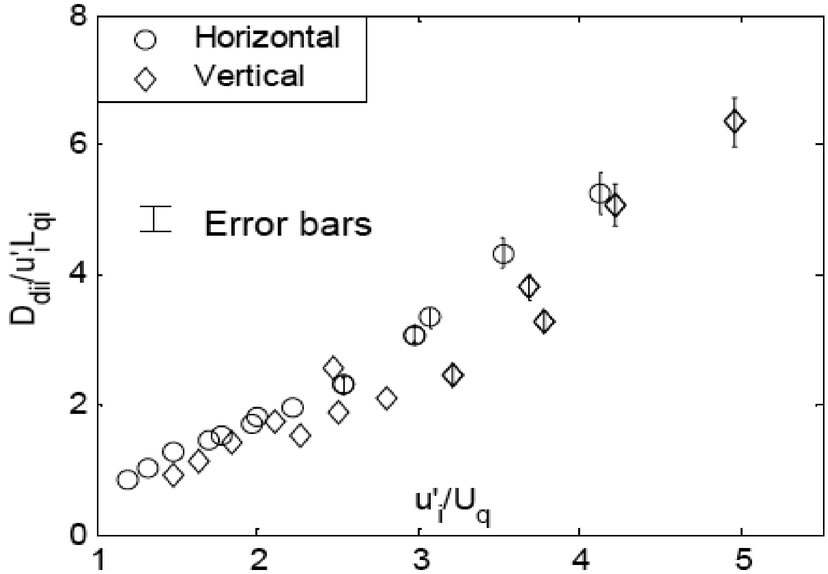

(a)

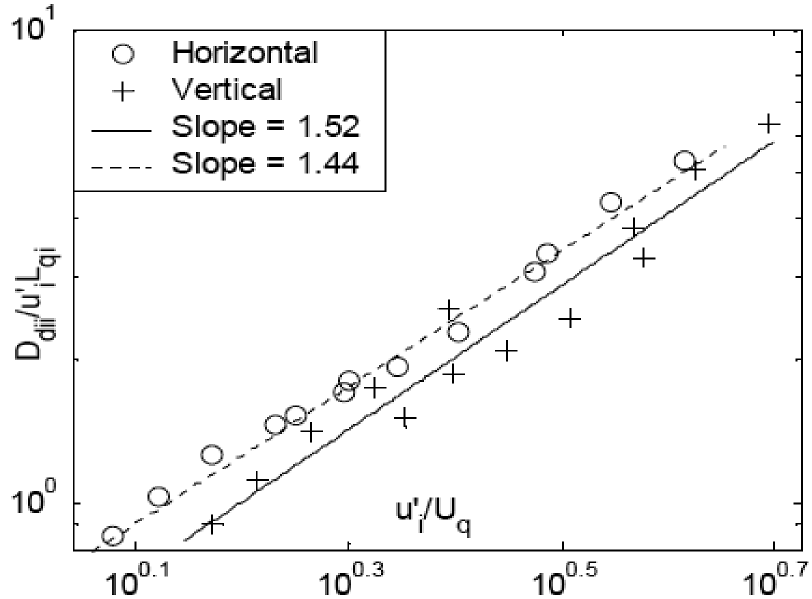

(b)

Figure 13: Variations, with u_i'/U_q, of the droplet horizontal and vertical diffusion coefficients normalized by $u_i'L_{qi}$ in (a) linear and (b) log scales.

$u_i'/U_q \ll 1$ (large droplets or low turbulence levels), following Csanady (1963), and neglecting the difference between Eulerian and Lagrangian length scales, we get $D_{dii} = u_i'^2 L / U_q$.

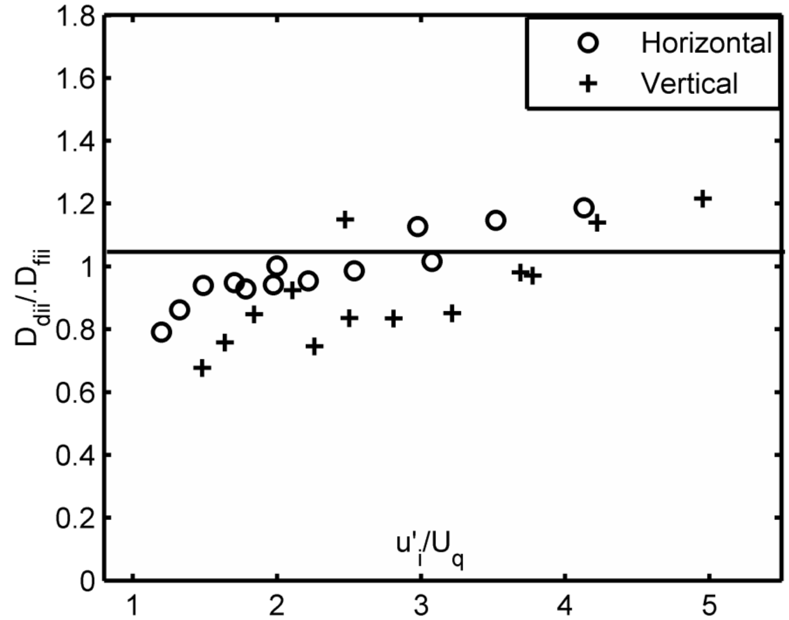

Figure 14: Droplet horizontal and vertical diffusion coefficient normalized by the corresponding fluid diffusion coefficient.

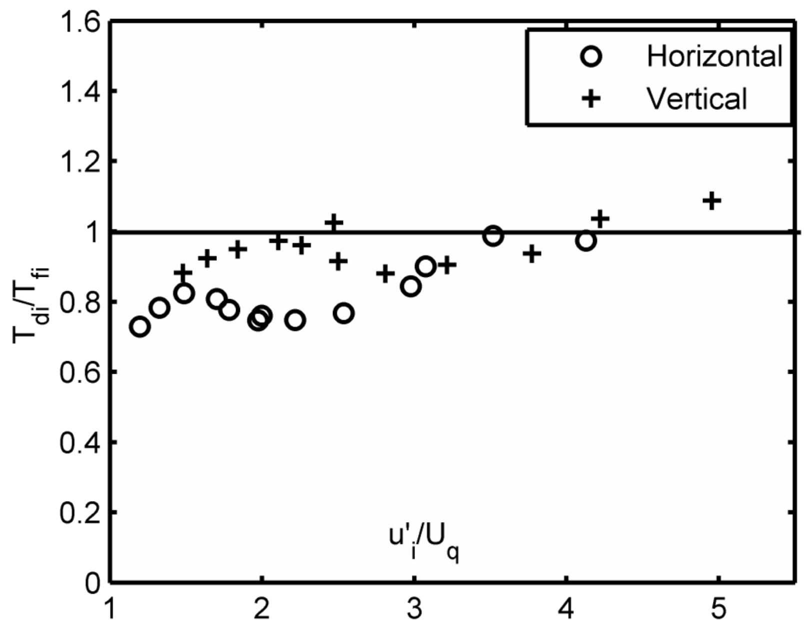

Figure 15: Droplet horizontal and vertical diffusion time scales normalized by the corresponding fluid diffusion time scales.

4.1.5 Droplet Diffusion vs. Fluid Diffusion

Figure 14 and 15 show the diffusion coefficient and timescale of the droplet normalized by the corresponding diffusion coefficient timescale of the fluid as a function of u_i'/U_q. It is evident that at low turbulence levels and/or large droplet size, i.e. $u_i'/U_q < 3$, the droplet diffusion coefficients, in both directions, are significantly lower than those of the fluid. Recognizing that $D_{dii} = U_i'^2 T_{di}$, trends of both the rms values and the diffusion timescales affect D_{dii}. In the horizontal direction, $U_x'/u_x' > 1$, but T_{dx}/T_{fx} is substantially lower than 1, resulting in $D_{dxx} < D_{fxx}$. In the vertical direction, both the timescale and the velocity fluctuations are lower than those of the fluid at low u_i'/U_q, each contributing to $D_{dyy} < D_{fyy}$. When $u_i'/U_q > 3$, D_{dxx} first exceeds the corresponding fluid diffusion coefficient due to combined effects of increasing rms velocity and increasing diffusion timescale. For $u_i'/U_q > 4$ the vertical droplet diffusion coefficient also exceeds that of the corresponding fluid diffusion coefficient, again due to combined effects of increasing U_y'/u_y' and the droplet diffusion timescale. Overall, with increasing u_i'/U_q, the normalized horizontal and vertical directions, the droplet diffusion coefficients increase and become closer to each other, a trend that can also be observed from the two straight line fits in Figure 13 b. The normalized vertical droplet diffusion coefficient at $u_i'/U_q \sim 2.4$, which deviates significantly from the generally observed trend, represents the lowest Stokes number data (~ 1) that we have, and we cannot currently explain the reason for this behavior. The low Stokes number range (St<1) should be investigated further.

The other clear observation from Figure 14 is that for most of the present cases, the normalized droplet horizontal diffusion coefficient is higher than the vertical one. These trends are inconsistent with previously published data, both for heavy particles, e.g. numerical simulations by Squires and Eaton (1990) and for bubbles, e.g. the numerical simulations of Spelt and Biesheuvel (1997) and Mazzitelli and Lohse (2002), as well as experimental data reported by Poorte (1998). The discussion in the next section examines this issue.

4.1.6 Dispersion of Extremely Small Oil Droplets

The diffusion coefficient of 35-70 μm oil droplets at Re_λ = 190 is compared to the fluid diffusion coefficient in Figure 16a. Within the experimental uncertainty, the Lagrangian statistics of these droplets and fluid particles are identical and hence under the current turbulent conditions they can be treated as fluid particles. It should be noted here that since we reduce the field of view (increase magnification) to follow these small oil droplets in the volume, we create a slight bias for long time scales towards tracks with vertical and horizontal loops, which enable them to remain in our limited field of view for extended periods. This bias reduces the diffusion coefficient slightly. Figure 16b compares this diffusion coefficient with those of the larger oil droplets discussed before. We can see clearly that the predictions made in section 4.1.4 are confirmed, i.e. that the increase of diffusion coefficient with u_i'/U_q does not persist indefinitely, and at some point, trends are reversed at some point. To complete the picture and cover all the range possible in ocean waters, we need to fill the gap 5< u_i'/U_q <120.

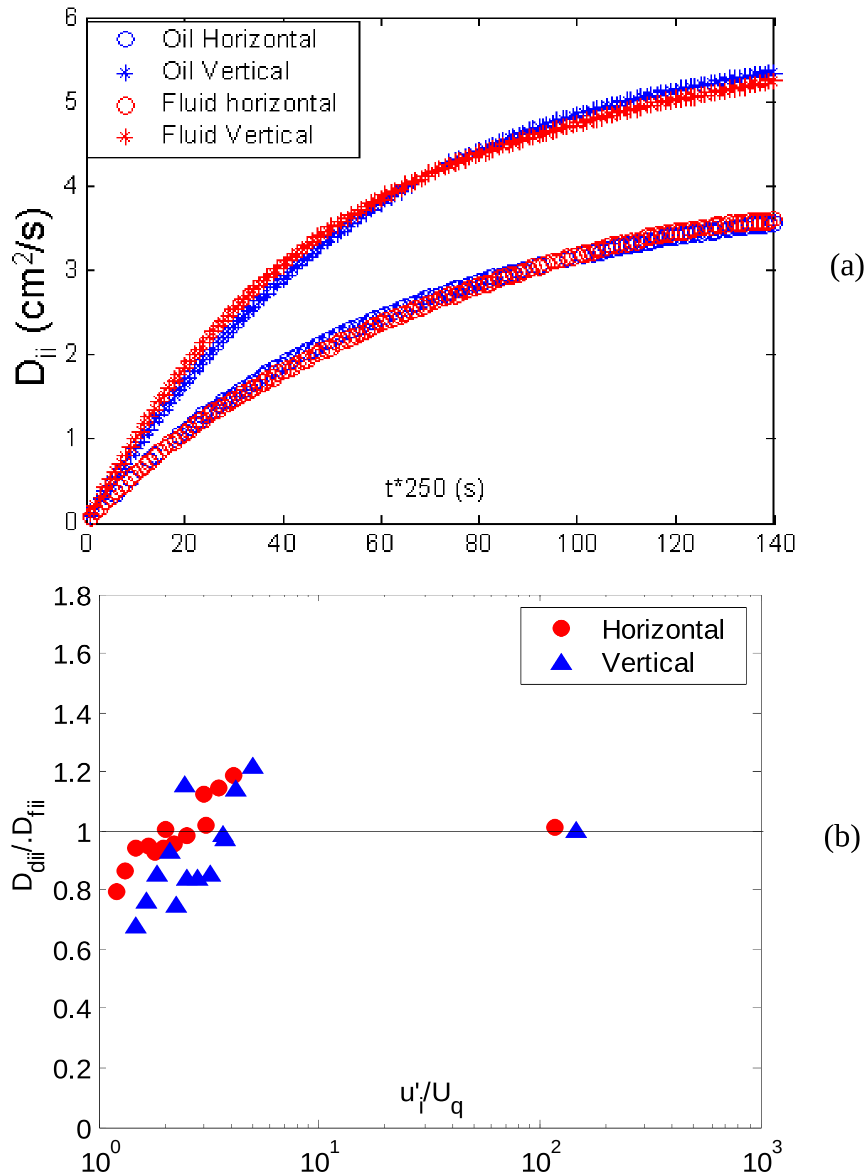

Figure 16: (a) Diffusion coefficient of 35-70 μm oil droplets compared to fluid particle dispersion (b) Droplet diffusion coefficient scaled by the fluid diffusion coefficient as a function of u_i'/U_q including 35-70 micron oil droplets.

4.1.7 Oil Droplet Mean Square Displacement

As discussed in the introduction, the droplet dispersion, i.e. mean square displacement, can be obtained by integrating the Quasi-Fickian diffusion coefficient (Equation 3).Figure 17 shows sample horizontal dispersions (X_{dx}^2) of 0.7-0.9 mm droplets for Re_λ = 214. As expected from Taylor's (1921) predictions, at short times, $X_{dx}^2(t) \propto t^2$, but at longer times the relation becomes linear.

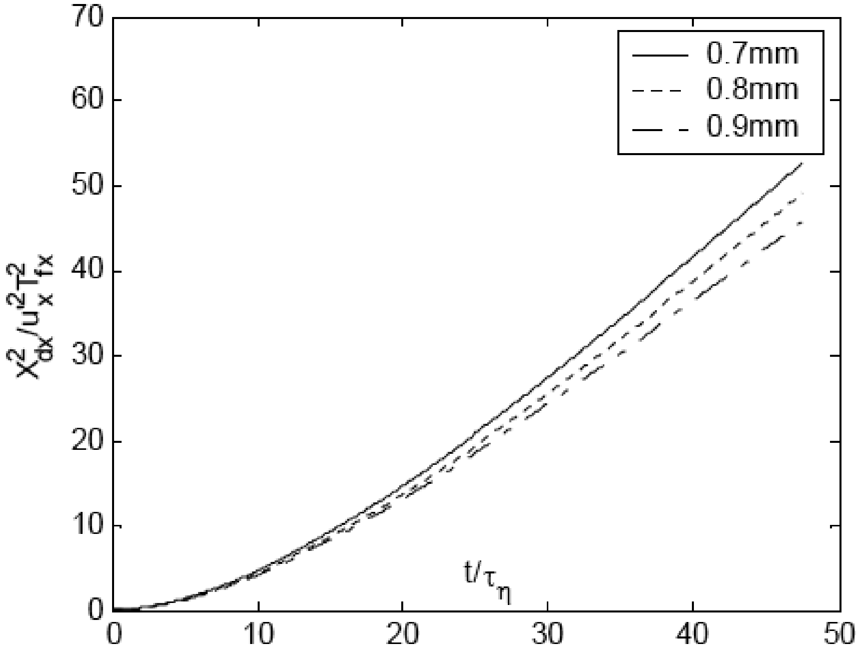

Figure 17: Sample droplet horizontal dispersion (mean square displacement) at Re_λ = 214.

4.2 Crude Oil Droplet Breakup

This part of the report deals with breakup of sample crude oil droplets, from Alaska National Slope, in the same turbulence facility. We first explain qualitatively the breakup process of the droplets by turbulence, and their relation to droplet and flow parameters. Then, we provide quantitative data on the droplet breakup in highly turbulent conditions. Finally, we explain the unique observation of formation micro-threads at high dispersant to oil ratios. The initial aim of these experiments is to obtain quantitative size distribution of daughter droplets for varying salinity, temperature, turbulence condition as well as Dispersant and oil properties. However the energetic level in the turbulence facility that we have used in the present study is not sufficient to break the crude oil droplets for all but the highest turbulence level, for which we have provided quantitative data (Higher turbulence levels are possible with minor modifications to the setup). When we tried varying the dispersant concentration to observe breakup at lower turbulence levels, we started observing a new mode of breakup, which to the best of our knowledge has not been reported before, that produces only extremely small, < 17 μm, droplets, our spatial resolution during the initial measurements. Hence, we decided to focus more qualitatively on this behavior and managed to combine our observations with more quantitative work performed by Li et al. (2007) to explain the formation of micro-droplets due to addition of dispersants. This phase of the project has not been completed. We have to quantify other modes of breakup at high turbulence levels, as well as the effect of turbulence level and oil-dispersant mixture properties on the formation of micro-droplets.

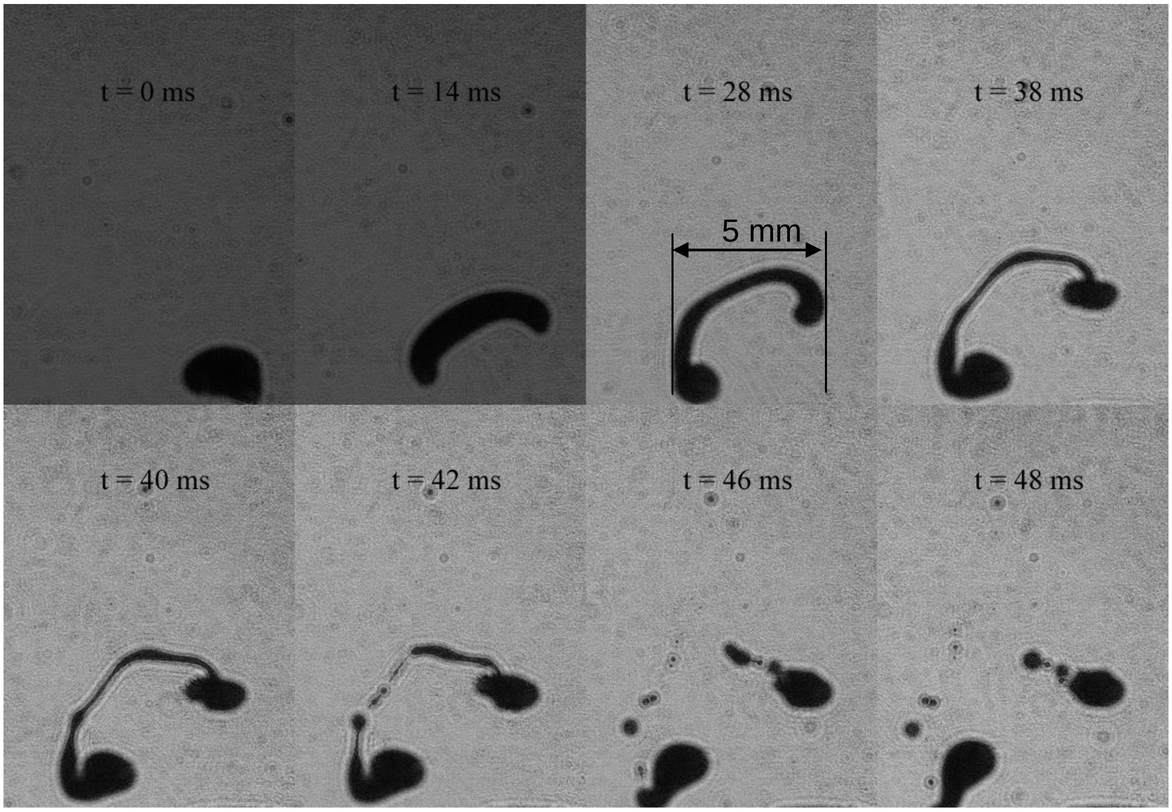

Figure 18: A sequence of 8 images showing breakup of a crude oil droplet mixed with dispersant. The timing is indicated on each image at Re_λ = 190

4.2.1 Qualitative Analysis of Droplet Breakup Process

A series of images showing the breakup process of a 2.3 mm droplet with DOR of 1:20, at Re_λ=190, is presented in Figure 18. The Weber number based on the droplet diameter, $We = \rho_w (\varepsilon d)^{2/3} d / \sigma$,where ρ_w is the density of water, σ is the interfacial tension and ε is energy dissipation rate due to the turbulence, is ~ 0.81. As the ratio of droplet to fluid viscosity is high, ~ 6, the effect of turbulence is to stretch the droplet to more than twice its initial diameter after 28 ms. Subsequently, after 38 ms, we can clearly observe formation of surface undulations of magnitude comparable to local thickness of the droplet. The actual breakup takes place about 42 ms after the droplet injection into the turbulence, about twice the Kolmogorov timescale. It is also evident that the primary breakup event at 42 ms is accompanied by secondary breakup events at 46 to 48 ms. The final breakup happens primarily due to capillary instability, similar to breakup of a liquid jet in air. The time elapsed to the actual breakup after the initial undulations occur is about 4 ms, 10% of the stretching time. Hence, the overall breakup time consists of both stretching time, probably governed by inertial and large scale turbulence, and a breaking time that is governed by capillary timescales.

The initial objective of these experiments has been to inject the droplets under quiescent conditions and then observe the time history of their deformation and subsequent breakup after entrainment under different turbulent conditions. However when the experiment is repeated at

Re_λ= 214, the droplets are already stretched when they enter the field of view. Hence, with the presently available data, we are unable to look at the effect of Reynolds number on the breakup time scales (To determine these time scales, we need to modify the procedures, which we hope to perform in future experiments). However, we can still observe the undulations in the stretched portion of the droplet, as shown in Figure 19, suggesting that the breakup mechanism is similar. In this figure, the reference time t = 0 ms does not have any physical significance, contrary to Figure 18, and serves only as a convenient reference point in the explanation of the breakup

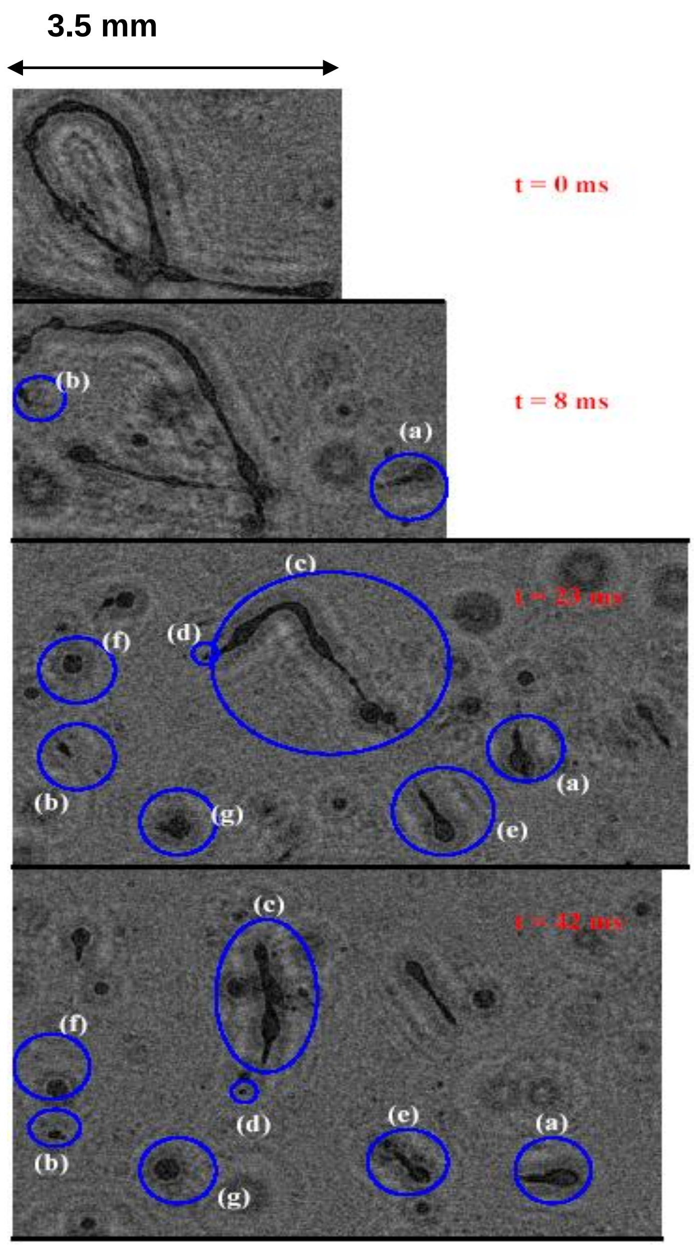

Figure 19: Snapshots of breakup of a stretched droplet at Re_λ= 214. Timing is indicated on each Figure.

process. The same droplets are marked by the same symbols in subsequent images.

The unique behavior of this breakup process, which we have not seen reported before, is the existence of tails trailing behind the bulbous droplet head. Clearly, the tail does not recoil into the head after a segment of the droplet breaks up. This consistent phenomenon can be clearly observed following droplets (a), (b) and (e), for which, even after 19-34 ms, the droplets still retain the elongated shape. This shape of droplets, that persists at least until the droplets leave our field of view, is probably a result of the extremely low surface tension caused by the addition of dispersants. The sharp edges of these extended droplets can breakup into even smaller droplets, e.g. formation of droplet (d) when the tail of droplet (c) breaks up. Though this type of breakup looks similar to tip streaming in an extensional flow (Sherwood, 1983) we currently do not have enough data to ascertain it. Furthermore, not all droplets have an extended shape as can be seen from sections (g) and (f) in Figure 19.

4.2.2 Size Distribution Associated with Capillary Droplet Breakup

Figure 20 shows the size distribution of daughter droplets, as measured during 25 different breakup observations, which are almost spherical in shape. We know from Rayleigh (1880) that a cylindrical stretch of liquid is unstable to wavelength greater than its size. We can also clearly see that daughter droplets size distribution peaks around 1 to 2η. However, the actual breakup happens due to capillary instability, which has no connection to length scales of turbulence, leaving us puzzled. To explain this trend, we realize that turbulence may affect this process by dissipating and/or stretching any perturbation before they grow, thereby preventing the breakup. Following this logic, breakup would occur when the time scale for capillary breakup is smaller than the timescales of continuous fluid flow phenomenon with sufficient energy to stabilize the capillary waves. For the breakup, we can use the capillary time scale, $\mu d / \sigma$, (Eastwood et al., 2004), which is ~1.5 ms for the median size of the daughter droplets. Hence, as the capillary timescale becomes comparable/smaller than the Kolmogorov time scale (6 ms for these experiments, see Table 1), the continuous fluid is unable to damp any further oscillations, and when this scale is reached, breakup occurs. Thus, we conjecture that the influence of Kolmogorov scale on the size of crude oil droplets treated with dispersants is a results of the stabilizing role of turbulent eddies, rather than the breakup role, as envisioned by Hinze (1955). Hence the effect of turbulence on the breakup process is twofold: First, large scale structures stretch and deform of the parent droplet, creating conditions favorable for capillary instability. Second, small-scale turbulent structures dissipate the oscillation along the surface of the strings by stretching them, thereby indirectly affecting the final size distribution. However, these postulates need to be confirmed/tested and challenged before accepting them. Note that if we are correct, there might be situations of viscous/capillary oil breakup where the size distribution has little relation to the Kolmogorov scale. Currently we have not included the droplets with extended shapes as we do not have the 3-D view to obtain the exact volume since 2-D projection varies with orientation size depends on the orientation relative to the camera. The size of most of these droplets is more than twice the Kolmogorov length scale, and their inclusion might make the distribution less skewed. This part of the project requires significant additional work.

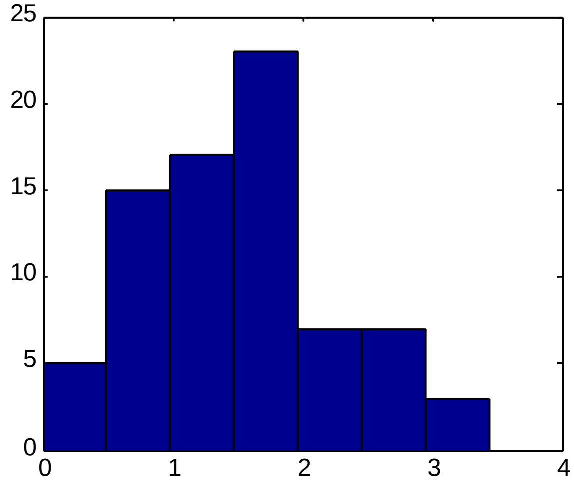

Figure 20: Size distribution of daughter droplets during capillary crude oil breakup, Re_{λ}= 214.

4.2.3 Formation and Breakup of Droplet Threads in Turbulent and Quiescent Flow

When a ~1mm droplet mixed with dispersant, at DOR of 1:15 to 1:18,enters the turbulent flow, portions of it are already stretched into small thread-like structures. As noted before, under the conditions tested to-date, the turbulence does not have the strength/intensity to stretch the entire droplet, resulting in its breakup, as observed by, e.g. by Eastwood et al. (2004) for the breakup of a viscous fluid blob. However, the small thread like structures are stretched by the turbulence into extremely long, well longer than 1 cm, thin threads, whose thickness quickly becomes smaller than the spatial resolution of our imaging system (~17 μm), hence they reach aspect ratio of more than 600. Contrary to the droplet, that does not follow the fluid particle motion, the threads are expected to be convected by the turbulence. Hence, we believe that the slip experienced by the droplet, which might be amplified under certain flow condition, e.g. as it is subjected to pressure gradients induced by eddies, is primarily responsible for producing the strain that stretches the threads. This conjecture is supported by the observation that the threads are not pulled continuously but rather intermittently. However, turbulence-induced differences in the local velocity along the thread may also affect the thread stretching, especially once the size of the threads becomes long enough to be affected by energetic large scale flow structures. Thus, the long threads extend almost continuously and frequently become twisted until sections of them get cut off. Figure 21 shows a typical time evolution of a thread being pulled from the droplet. These threads, though thin, are very stable, and when a thread separates from the droplet, it leaves behind a portion, which acts as seed for the future threads, making this process self sustaining. The stability of these threads stem from the high viscosity of the droplets, low interfacial tension and the extension/stretching of the threads that dissipates any interfacial oscillations before they grow.

Though we have not yet observed the threads breaking up into droplets in turbulent flow, due to the limited spatial resolution of experiments performed to-date (the sample volume is located far from the window, see Figure 1, limiting the magnification to 17μm/pixels), one can predict that eventually these threads breakup to micron size droplets. There are several contributors to this breakup. During early stages of stretching, the surfactant concentration near the surface increases with decreasing size of the threads due to increasing gradients within the thread that enhances the flux towards the interface. As the thread becomes thin and time elapses, diffusion of surfactant into the water starts reducing its concentration within the droplet. This effect becomes significant when the diffusion length scale exceeds the radius of the thread after ~0.2 s.

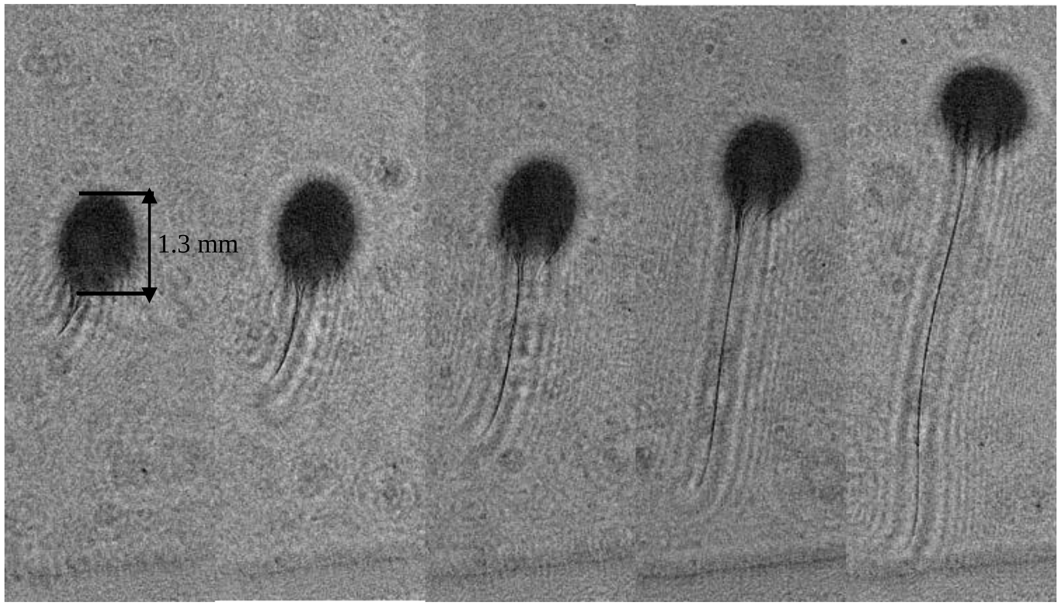

Figure 21: Extension of a thread from droplet upon entering the turbulent flow region. Delay between time steps is 20 ms.

As a result, the interfacial tension starts increasing, causing breakup due to capillary instability. Alternatively, one can argue that the timescale of stretching might become larger than the timescale it takes for the instabilities to grow and hence the thread breaks. Some of the threads are pulled from these droplets without any pre-existing small extensions, indicating that formation of the threads is not necessarily an outcome of the droplet injection process. The observation of thread separation and formation of micro droplets in the quiescent conditions, Figure 23 a, justifies this explanation.

Janssen et al. (1997) studied the influence of surfactants on droplet deformation and breakup in a plane hyperbolic flow experimentally in an opposed-stream device. Though the threads from these droplets have some qualitative similarity with the asymmetric end pinching, originally/first observed by Janssen et al. (1997), there are significant differences. In “asymmetric end pinching” the entire droplet is stretched into an elliptical shape initially. Then a portion of it is stretched further to a thread like structure while the remaining portion retracts back to a spherical surface, as can be clearly seen in Hu et al. (2000). Hence, the final shape looks similar to our current droplet with threads. However, in the present case, only a local region along the interface is affected when the threads are being pulled, even for cases which do not have pre-existing structures. In addition, there is no daughter droplet pinching off from the tail, and the breakup, when it happens, is due to capillary instability. Although the formation of very long threads or their stability are unexpected, a particularly intriguing part of this process is the non-retraction of the portion of thread remaining attached to the droplet after breakup, which makes this process self sustaining and long lasting. Note that the droplet in Figure 21 has several short threads extending from its back, with only one of them extends significantly. Also, depending on the local turbulence conditions, multiple threads can also be pulled from droplets simultaneously, as demonstrated in Figure 22. Because it is self-sustaining, this process becomes a dominant mechanism for small droplets formation during breakup of an oil spill, as will be shown shortly.

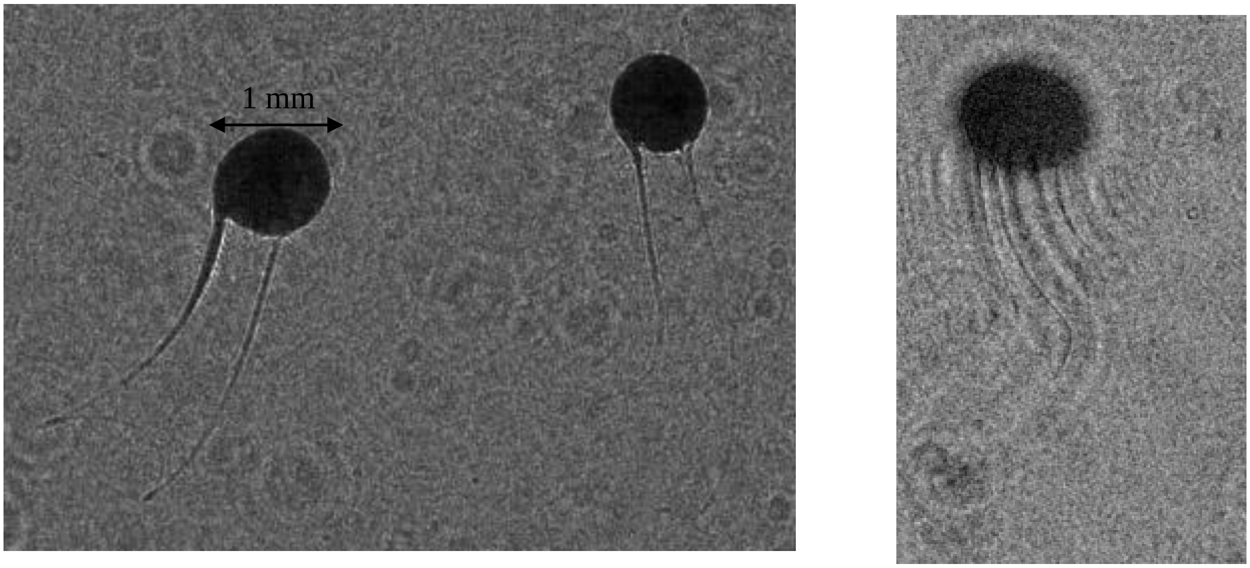

(a) (b)

Figure 22: Droplets with multiple (a) two and (b) three threads extension in isotropic turbulence flow.

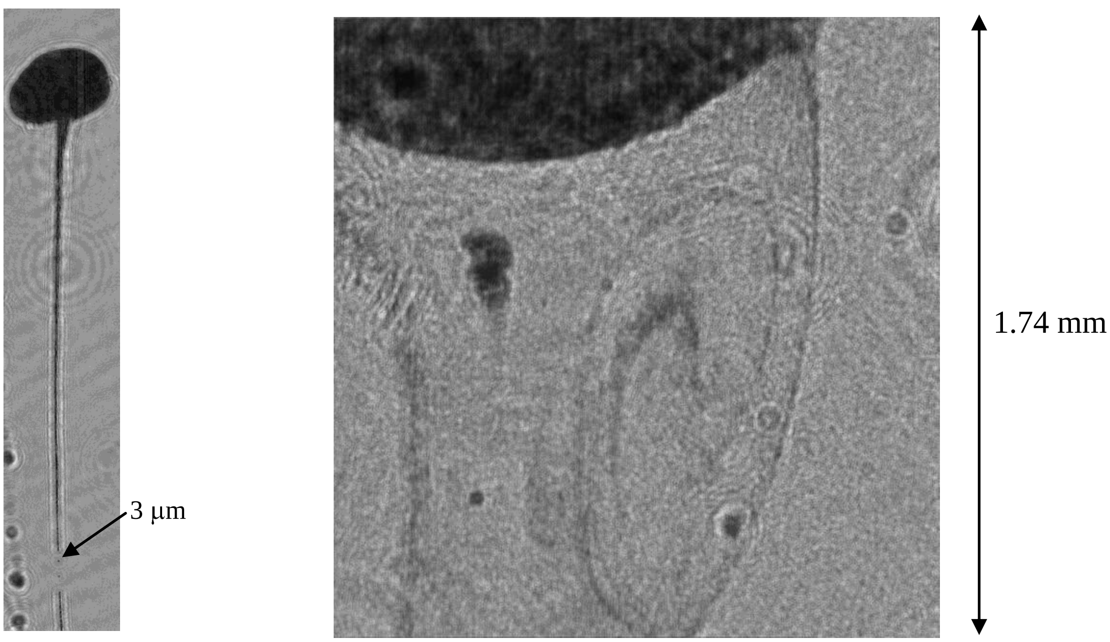

(a) (b)

Figure 23: Formation of a droplet with a long thread extending from it, and breakup of this tail to 3 μm droplets, DOR=15. (b) Formation of an axisymmetric tail extending from the point of flow separation on the surface of the droplet, DOR=18. In both cases, crude oil mixed with dispersant is injected into quiescent fluid.

To examine and understand the thread-formation process and its breakup to micro-droplets, we have also performed droplet injection experiments in quiescent conditions, which simplify observations at high magnification. Injection of a droplet from a nozzle/needle is a very complicated process, which depends on several parameters including needle size, injection rate, viscosity of fluids, interfacial tension and presence of surfactants, etc. (Webster and Longmire, 2001). When the crude oil mixed with dispersants, at DOR ranging from 1:20 to 1:15, is injected using a hypodermic needle into a quiescent region and observed using a 2k x 2k digital camera at 5X magnification, we observe two modes of injection. When the dispersant to oil ratio is 1:18, axi-symmetric shedding seems to occur along the line of boundary layer separation on the surface of the droplet, as shown in Figure 23b. As separation occurs, oil and dispersant might be sheared away from the surface, leading to formation of threads, as the droplet migrates upward due to gravity.

When the dispersant to oil ratio is increased to 1:15, as in Figure 23a, a thin thread extends from the tail of the droplet and connects it to the oil in the needle, similar to Doshi et al. (2003) for injection of low viscosity water droplets into highly viscous silicone oil. As the droplet rises, this thread become thinner, eventually breaking from the needle, while remaining attached to the droplet. As explained by Jin et al. (2006), any sudden contraction in the thread inherently involves an increase in the pre-mixed surfactant concentration on the surface, causing an exponential decrease in interfacial tension. Their simulation of the detachment of a viscous drop in a viscous solution in the presence of a soluble surfactant shows that for extremely low surface tension, the eventual breakup of the thread occurs near the needle such that a portion of the thread remains with the droplet. We observe that the portion of the thread remaining attached to the droplet does not retract after the breakup, and believe that this process causes the formation of the initially extended tails, when the droplets emerge from the tube and enter the turbulent flow during the experiments in the isotropic turbulence facility. The threads in quiescent flow eventually break down into extremely small droplets due to capillary instability, as small as 3 μm in our experiments (Figure 23a). We believe that this process plays a key role in formation of micro-droplets in flask bottle experiments involving crude-oil droplets mixed with dispersants. Because of its significance and sensitivity to dispersant concentration and flow mechanisms causing the shearing, the present work provides only preliminary results, which identify the basic mechanism involved. This effort should be extended to careful characterization of droplet sizes as a function of turbulence level, as well as surfactant concentration and properties.

4.2.4 Connection to Actual Oil Spill Scenario

We also believe that the present observations are directly connected to phenomena occurring during actual oil spill breakup and formation of micro droplets due to dispersant addition that were observed by Li et al. (2007) and Lee et al. (2007). During their experiments in a wave tank facility, which mimicked an oil spill breakup, they observed that addition of surfactants produced a bimodal distribution of droplets. The first with droplets in the 10 - 500μm size range, and the second, distinctly different mode, consisting of droplets, ranging from 1-4 μm in diameter. Without additions of surfactants the size distributions have single modes for regular, spilling and plunging breaking waves, ranging in size from 50 to 400 μm. The size of droplets that we have obtained during quiescent breakup of the thin threads is very close to that of the second mode, suggesting that the 1-4 μm droplets are generated by capillary instability of extended micro-threads. These micro droplets, along with the larger ones observed in Figures 18-20, which are formed due to turbulent stretching of the entire parent droplet and subsequent capillary breakup, explain the bimodal distribution of droplet size. To confirm our hypothesis we have conducted model experiments, during which a layer of oil mixed with dispersants is impacted with drops of water to simulate the impact of a breaking wave. As illustrated in Figure 24, our visualization clearly demonstrates formation of numerous, very long thin filaments extending from larger droplets, whose appearance is very similar to that of the threads forming in the turbulent flow, and during injection into a quiescent fluid. As the larger droplets floating on the surface are forced to move, the threads/tails extend in time, presumably breaking up eventually to micron-size droplets as capillary instabilities eventually take over. However, the threads persist, making the process self-sustaining. At this phase of the project, the latter statements are qualitative, and require quantitative measurement of droplet sizes as a function of impact loads by the impinging water, oil and dispersant properties.

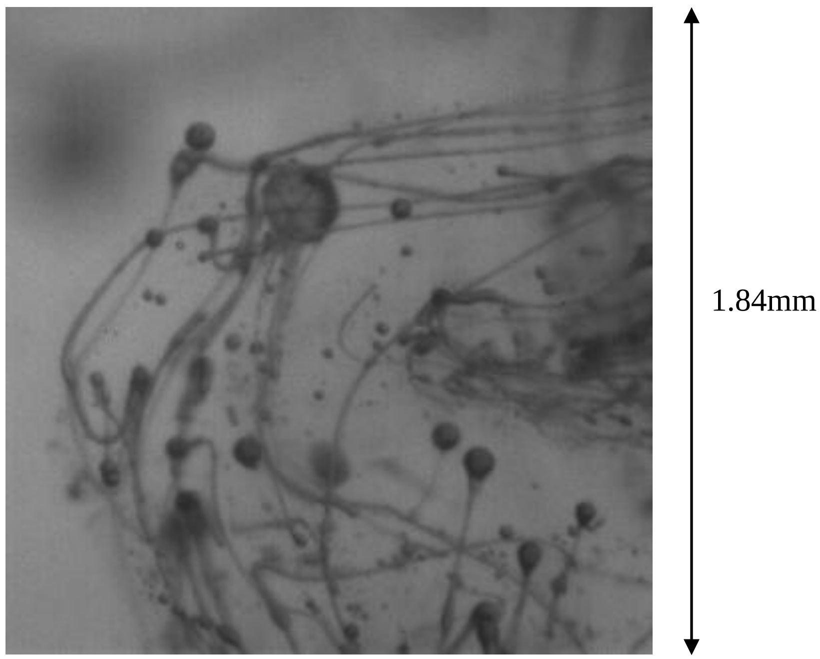

Figure 24: Formation of droplet with very long threads extending from them when a jet of water impinges a surface layer containing oil mixed with dispersant.

5.0 Importance to Oil Spill Response/Restoration

- This project provides statistics and resulting empirical relations for oil droplet dispersion and rise velocity as a function of turbulence and droplet parameters. Besides the fundamental insight, results are expressed in a format that can be implemented in computational models of, e.g. oceanic turbulent flows in order to predict the fate of oil droplets generated as an oil spill is treated with dispersants.
- Careful observations on droplet breakup demonstrate that two distinctly different processes and associated time scales and droplet sizes affect the viscous droplet breakup. This effort should be followed by detailed characterization of droplet size distributions generated by each process, and parameters affecting them, such as dispersant properties, viscosity ratio, surface tension and characteristics of the process generating the droplets. These data are essential for modeling of the fate of oil spills treated with dispersants.

- Our results reveal that the low surface tension of oil mixed with dispersants creates unique self-sustaining phenomenon that generate extremely small droplets.

6.0 Technology Transfer

- Results of the dispersion section have already been published in a Journal paper and in a series of conference papers.
- A journal publication focusing on the sections dealing with oil droplets breakup has been submitted to Physical Review Letters. Conference papers and presentations containing parts of the data have already been published/presented.
- The PhD thesis of graduate student Balaji Gopalan, which is presently being prepared, contains all the relevant data and figures.
- The raw and processed data are also available upon request to any researcher who needs it for validation or model development. Prof Murray Snyder from the US Naval Academy has already used our data as a basis for comparisons with numerical predictions of rise velocity of droplets (Snyder et al., Phys. Of Fluids, 20, 073301).
- Results have been made available to Bill Lehr from NOAA for inclusion in their oil dispersion models.
- The hologram reconstruction and tracking programs that have been developed in part under this program have been made available to other groups, and have already been utilized by groups in Louisiana State University and Rutgers University.

7.0 Achievement and Dissemination

Journal Paper

Gopalan, B., Malkiel, E. and J. Katz. 2008. Experimental Investigation of Turbulent Diffusion of Slightly Buoyant Droplets in Isotropic Turbulence. Physics of Fluids20: 095102.

Conference Papers

Gopalan, B., Katz, J. 2008. Break up of Viscous Crude Oil Droplets Mixed with Dispersants in Locally Isotropic Turbulence. FEDSM2008-55165,Proceedings of ASME Fluids Engineering Conference, August 10-14, Jacksonville FL.

Talapatra, S., Hong, J., Sheng, J., Waggett, B., Tester, P. and Katz, J. 2008. A Study of Grazing Behaviors of Copepods Using Digital Holographic Cinematography, FEDSM2008-55196, Proceedings Of ASME Fluids Engineering Conference, August 10-14, Jacksonville FL.

Gopalan, B., Malkiel, E. and J. Katz. 2007. Lagrangian Motion of Slightly Buoyant Droplets and Fluid Particles in Isotropic Turbulence. Paper No. FEDSM2007-37538, Proceedings Of FEDSM2007, Joint ASME/JSME Fluids Engineering Conference, July 30-August 2, San Diego, CA.

Gopalan, B., E. Malkiel, and J. Katz. 2007. Lagrangian Statistics of the Motion of Slightly Buoyant Droplets in Isotropic Turbulence. 6th International Conference on Multiphase Flow, ICMF 2007, Leipzig, Germany, July 9 – 13.

Conference Abstracts and Presentation

Gopalan, B., and J. Katz. 2008. Formation of Long Tails during Breakup of Oil Droplets Mixed with Dispersants in Locally Isotropic Turbulence. Abstract # MH.00004, 61st Annual Meeting of the APS Division of Fluid Dynamics, November 23–25, San Antonio, Texas.

Talapatra, S., Hong, J., Lu, Y. and J. Katz. 2008. Microscopic Holography for Flow Over a Rough Plate. Abstract # GT.00008, 61st Annual Meeting of the APS Division of Fluid Dynamics, November 23–25, San Antonio, Texas.

Gopalan, B., Malkiel, E., Karp-Boss, L., Sheng, J. and J. Katz. 2008. Diffusion of Particles in Isotropic Turbulence Using High Speed Digital Holographic Cinematography. Abstract # 3210, AGU-ASLO Ocean Science Meeting, March 2-7, Orlando FL.

Gopalan, B., E. Malkiel, and J. Katz. 2007. Experimental Investigation of Lagrangian Statistics of Motion of Diesel Oil Droplets and Fluid Particles in Isotropic Turbulence. Abstract No. BT.00001, 60th Annual Meeting of the Division of Fluid Dynamics of APS, November 18–20, Salt Lake City, Utah.

Sheng, J., Gopalan, B., Malkiel, E. and J. Katz. 2007. Measurements 3D Flow and Particle Motion in the Laboratory and in the Ocean Using Digital Holography (Holographic Microscopy). Seminar on Experimental Fluid Mechanics, Computer Vision & Pattern Recognition, March 18-23, Schloss Dagstuhl, Germany.

8.0 References

Batchelor, G.K. 1950.Diffusion in a field of homogeneous turbulence. I. Eulerian analysis, Australian Journal of Scientific Research 2(4): 437-450.

Colin, C. and D. Legendre. 2001. Bubble distribution in turbulent shear flows: experiments and numerical simulations on single bubbles. Proceedings of Fourth International Conference on Multiphase Flow: 1–12.

Crowe, C.T., Sommerfeld, M. and Y. Tsuji. 1998. Multiphase flows with droplets and particles. CRC Press.

Csanady, G.T. 1963. Turbulent diffusion of heavy particles in the atmosphere. J. Atmos. Sci. 20: 201.

Deng, F.W. and J.H. Cushman. 1995.Comparison of moments for classical-, quasi-, and convolution-Fickian dispersion of a conservative tracer. Water Resources Research 31(4): 1147-1149.

Doshi, P., Cohen, I., Zhang, W.W., Siegel, M., Howell, P., Basaran, O.A. and S. R. Nagel. 2003. Persistence of memory in drop breakup: The breakdown of universality. Science 302: 1185.

Eastwood, C.D., Armi, L. and A.C. Lasheras. 2004. The breakup of immiscible fluids in turbulent flows. Journal of Fluid Mechanics, 502: 309-333.

Eastwood, C.D. 2002. . The breakup of immiscible fluids in turbulent flows. PhD Thesis. University of California, San Diego.

Eggleton, C.D., Tsai, T.-M. and K. J. Stebe. 2001. Tip streaming from a drop in the presence of surfactants. Phys. Rev. Lett. 87: 048302.

Friedman, P.D. and J. Katz. 2002. Mean rise rate of droplets in isotropic turbulence. Physics of Fluids 14: 3059-3073.

Grace, H. P. 1971. Dispersion phenomena in high viscosity immiscible fluid systems and

application of static mixers as dispersion devices in such systems. Eng. Found. Res. Conf. Mixing, 3rd, Andover, N. H. Republished in 1982 in Chem. Eng. Commun.4:225-77.

Hinze, J. O. 1955. Fundamentals of the hydrodynamics mechanisms of splitting in dispersion process. AIChE J. 1: 289–295.

Hu, Y.T., Pine, D.J. L.G. Leal 2000. Drop deformation, breakup, and coalescence with compatibilizer. Phys. Fluids 12: 484.

Janssen, J. J. M., Boon, A. and W.G.M Agterof. 1997. Influence of dynamic interfacial properties on droplet breakup in plane hyperbolic flow. AIChE. J.43: 1436–1447.

Jin, F., Gupta, N.R. and K. J. Stebe. 2006. The detachment of a viscous drop in a viscous solution in the presence of a soluble surfactant. Phys. Fluids18: 022103.

Li, Z., Kepkay, P., Lee, K., King, T., Boufadel, T. and A.Venosa. 2007. Effects of chemical dispersants and mineral fines on crude oil dispersion in a wave tank under breaking waves. Marine Pollution Bulletin54(7): 983-993.

Lee, K., Venosa., A., Boufadel, T. and M.S., Miles 2007. Wave Tank Studies on Dispersant Effectiveness as a Function of Energy Dissipation Rate and Particle Size Distribution. Technical Report Submitted to CRRC, April.

Lessard, R.R. and G. Demarco. 2000. The Significance of Oil Spill Dispersants. Spill Science and Technology Bulletin6: 59-68.

Malkiel, E., Sheng, J., Katz, J. and J.R. Strickler. 2003. Digital holography of the flow field generated by a feeding calanoid copepod, diaptomus minutus. Journal of Experimental Biology 206: 3657-3666.

Mazzitelli, I.M. and D. Lohse. 2003. Lagrangian statistics for fluid particles and bubbles in turbulence. New Journal of Physics 6: 203.

Meng, H. and F. Hussain. 1991. Holographic particle velocimetry - A 3D measurement technique for vortex interactions, coherent structures and turbulence. Fluid Dynamics Research 8: 33-52.

Milgram, J.H. and W. Li. 2002. Computational reconstruction of images from holograms. Optical Soc. of America 41: 853-864.

Morales, R.A., Elliott, A.J. and T. Lunel. 1997. The influence of tidal currents and wind on mixing in the surface layers of the sea. Marine Pollution Bulletin 34: 15-25.

Mordant, N., Metz, P., Michel, O. and J.-F. Pinton. 2001. Measurement of Lagrangian velocity in fully developed turbulence. Phys. Rev. Lett., 87(214501): 1-4.

Poorte, R.E.G. and A. Biesheuvel. 2002. Experiments on the motion of gas bubbles in turbulence generated by an active grid. Journal of Fluid Mechanics 461: 127-154.

Poorte, R.E.G.1998. On the motion of bubbles in active grid generated turbulent flows. Dissertation.

Pope, S.B. 2000. Turbulent Flows. Cambridge University Press.

Rayleigh Lord. 1880. On the Stability, or Instability, of certain Fluid Motions. Proc. Lond. Math. Soc. 1: 57.

Reeks, M.W. 1963. On the dispersion of small particles suspended in an isotropic turbulent fluid. Journal of fluid mechanics 83: 529-546.

Roth, G. and J. Katz. 2001. Five techniques for increasing the speed and accuracy of PIV interrogation. Meas. Sci. Technol. 12: 238.

Sato, Y. and K. Yamamoto. 1986. Lagrangian measurement of fluid-particle motion in an isotropic turbulent field. Journal of Fluid Mechanics 175: 183-199.

Sheng, J., Malkiel, E. and J. Katz Single beam two-views holographic particle image velocimetry, Applied Optics, 42, 235 (2003).

Sheng, J., Malkiel, E. and J. Katz. 2006. A digital holographic microscope for measuring three dimensional particle distributions and motions. Applied Optics Journal 45: 3893-3901.

Sherwood, J.D. 1983. Tip streaming from slender drops in a nonlinear extensional flow. J. Fluid Mech.144: 281-295.

Snyder W.H. and J.L. Lumley. 1971. Some measurements of particle velocity autocorrelation functions in a turbulent flow. Journal of Fluid Mechanics 48: 41.

Snyder, M.R., Knio, O.M., Katz, J. and O.P. Le Maitre. 2006. Statistical analysis of small bubble dynamics in isotropic turbulence. Physics of Fluids 19(065108): 1-25.

Spelt, P.D.M. and A. Biesheuvel.1997. On the motion of gas bubbles in homogeneous isotropic turbulence. Journal of Fluid Mechanics 336: 221-244.

Spelt, P.D.M. and A. Biesheuvel. 1998. Dispersion of gas bubbles in large-scale homogenous isotropic turbulence. Applied Scientific Research 58: 463-482.

Squires, K.D. and J.K. Eaton. 1990. Measurements of particle dispersion obtained from direct numerical simulations of isotropic turbulence. Journal of Fluid Mechanics 226: 1-35.

Stone, H. A. and L.G. Leal. 1989a. Relaxation and breakup of an initially extended drop in an otherwise quiescent fluid. J. Fluid Mech.198:399-427.

Talbot, J.W. and G.A. Talbot. 1974. Diffusion in shallow seas and in English coastal and estuarine waters. Rapp. P.-v. Reun. Cons. int. Explor. Mer.167: 93-110.

Tao, B., Katz, J. and C. Meneveau. 2002. Statistical geometry of sub-grid scale stresses determined from holographic particle image velocimetry measurements. Journal of Fluid Mechanics 457: 35-78.

Taylor, G.I.1921. Diffusion by continuous movements. Proc. London Math. Soc. 2: 196-211.

Wang, L.P. and M.R. Maxey. 1993. Settling velocity and concentration distribution of heavy particles in homogeneous isotropic turbulence. Journal of Fluid Mechanics 256: 27-68.

Webster, D.R. and E. K. Longmire. 2001. Jet pinch-off and drop formation in immiscible liquid-liquid systems. Exp. Fluids 30: 47.

Wells, M.R. and D.E. Stock. 1983. The effects of crossing trajectories on the dispersion of particles in turbulent flow. Journal of Fluid Mechanics 136: 31-62.

Zhang, X. and O.A. Basaran. 1995. An experimental study of dynamics of drop formation. Phys. Fluids 7: 1184.